Summary

Purpose of the Research

Residential air handling units (AHUs) have stayed the same in form and efficiency for the past 30+ years, with incremental improvements made to address safety, functionality, and energy-efficiency. The purpose of this research in Phase I, Topic 9a: Next Generation Residential Air Handlers, was to improve AHU performance by minimizing heat exchanger (HX) approach temperature, reducing air maldistribution, and developing alternative system configurations which more efficiently handle sensible and latent loads.

Brief Description of the Research

In this research Optimized Thermal Systems (OTS) developed, modeled, and evaluated multiple alternative system concepts. A dual vapor compression system separate sensible and latent cooling (SSLC) concept was studied to inform work on alternative concepts and to show best-case performance benefit. System concepts included ejector enhanced vapor compression cycles, desiccant assisted dehumidification, dual evaporator SSLC, and alternative AHU HX configurations.

Research Findings

A dual vapor compression system showed COP improvement of 20%, however, required additional components, increased unit size, and increased cost. Two types of ejector enhanced vapor compression cycles with dual evaporators improved system COP by 9 to 11%, and reduced AHU losses by as much as 18%, with design changes limited to the AHU, no unit physical size increase, and a moderate increase to system first cost. Desiccant assisted air-conditioning required increased air flow rate resulting in higher fan power and the desiccant wheel increased sensible heat load leading to increased compressor power and reduced system COP. Dual evaporator cycles were found to degrade performance due to increased expansion losses. Optimized single slab HX designs used in place of the traditional A-coil HX led to 44–49% reduction in aluminum, 47–60% less refrigerant charge, and improved HX velocity distribution.

Potential Applications of the Research

OTS identified a design for a next generation residential AHU intended to reduce energy consumption and improve indoor comfort. The design would serve new construction market for single- and multi-family construction, as well as a retrofit unit for existing building stock. Superior to conventional AHUs the design leverages the benefits of an ejector and SSLC. Ejectors were found beneficial in this air conditioning application, yet commercial availability is poor, hindering adoption and potential integration into new systems. Future work on this topic will lead to potentially novel ejector designs, commercialization of the proposed AHU concept, and wider adoption of energy saving ejector technology.

Improving AHU Performance by Minimizing Approach Temperature, Reducing Air Maldistribution, and Efficiently Handling Sensible and Latent Loads

SBIR Phase I Interim Final Technical Report
Topic 9a: Next Generation Residential Air Handlers, DE-FOA-0001941

Prepared for the United States Department of Energy

June 30, 2020

Lead Organization:
Optimized Thermal Systems, Inc. (OTS)

Team Members:
Goodman Manufacturing Company, L.P.

Principal Investigator:
James Carow carow@optimizedthermalsystems.com

Business Point of Contact:
Cara Martin cmartin@optimizedthermalsystems.com

Table of Contents

List of Figures

List of Tables

List of Acronyms & Abbreviations

AC	Air-Conditioning
AHRI	Air-Conditioning, Heating, & Refrigeration Institute
AHU	Air Handling Unit
BTO	Building Technologies Office
CFD	Computational Fluid Dynamics
CO_2	Carbon Dioxide
COP	Coefficient of Performance
COS	Condenser Outlet Split
DOE	Department of Energy
DOS	Diffuser Outlet Split
DW	Desiccant Wheel
EA	Exhaust Air
ECM	Electronically Commutated Motor
EER	Energy Efficiency Ratio
EES	Engineering Equation Solver®
EIA	Energy Information Administration
HSPF	Heating Seasonal Performance Factor
HVAC	Heating, Ventilation, and Air-Conditioning
HX	Heat Exchanger
k-ε	Turbulent kinetic energy – turbulent energy dissipation rate
LMTD	Log-Mean Temperature Difference
LWTD	Log-Mean Humidity Ratio Difference
OA	Outside Air
ODU	Outdoor Unit
OTS	Optimized Thermal Systems, Inc.
P-h	Pressure – enthalpy
PIV	Particle Image Velocimetry

RA	Return Air
RH	Relative Humidity
SA	Supply Air
SEER	Seasonal Energy Efficiency Ratio
SHR	Sensible Heat Ratio
SOS	Separator Outlet Split
SSLC	Separate Sensible and Latent Cooling
T-s	Temperature-entropy
TXV	Thermostatic Expansion Valve
VCS	Vapor compression system

Nomenclature

Symbol	Description	Units
A	Coil area	m^2
F	Source load function	-
F_{size}	Compressor scaling factor	-
h	Specific enthalpy	kJ/kg
$\dot{m}$	Mass flow rate	g/s or kg/s
n	Ejector pressure fraction	-
P	Pressure	Pa
$\dot{Q}$	Capacity	W
r	Ejector mass flow ratio	-
r_{comp}	Compressor speed ratio	-
r_{fan}	Fan speed ratio	-
r_p	Ejector pressure lift ratio	-
s	Specific entropy	kJ/kg-K
T	Temperature	°C
U	Overall heat transfer coefficient	W/m^2-K
V	Velocity	m/s
$\dot{W}$	Work input	W or kW
y	Evaporator capacity split	-

Greek Symbol	Description	Units
Δ	Delta (difference)	n/a
η	Efficiency	-
μ	Ejector entrainment ratio	-
μ_{evap}	Evaporator mass flow ratio	-
ϕ	Specific exergy	kJ/kg
$\dot{\phi}$	Exergy destruction rate	kW
ω	Humidity Ratio	kg/kg

Subscript	Description
a	Air
app	Approach
comp	Compressor
cond	Condenser
dest	Destroyed
diff	Diffuser
evap	Evaporator
ex	Exergy
h	Heat transfer coefficient
in	Inlet
m	Mass transfer
mix	Mixing
mn	Ejector motive nozzle
o	Dead (equilibrium) state
out	Outlet
pro	Process (Air)
reg	Regeneration (Air)
s	Isentropic
SC	Subcooling

Subscript	Description
SH	Superheat
sn	Ejector suction nozzle
tot	Total

Executive Summary

In Phase I, Topic 9a: Next Generation Residential Air Handlers, Optimized Thermal Systems, Inc. (OTS) focused on improving air handler unit (AHU) performance by minimizing heat exchanger (HX) approach temperature, found opportunities to reduce air maldistribution, and proposed and analyzed alternative system configurations which can more efficiently handle sensible and latent loads.

Goodman Manufacturing Company, L.P. (Goodman) acted as a technical and commercial consultant and advisor, assisting with the selection of the baseline, and providing input on the proposed technologies.

The goals for system performance, as specified by Department of Energy (DOE), included reducing the energy consumption of the AHU by 25% and reducing overall system energy consumption by 5%. System improvements could further not impose increased cost, complexity, or negative effects on reliability. To assess whether such goals were met, OTS focused its analysis on a single-speed, 3-ton Goodman AHU with accompanying condensing unit with a rated efficiency of 15 SEER.

The primary focus of the proposed technology concepts was to achieve separate sensible and latent cooling (SSLC).

OTS developed and evaluated multiple concepts in several solution categories: ejector enhanced vapor compression cycles; desiccant assisted dehumidification; dual-evaporator, SSLC; and alternative AHU HX configurations and designs. Results for each of these concepts are summarized as follows:

- A hypothetical dual vapor compression system (VCS) SSLC concept was studied to inform alternative concepts and to determine best-case theoretical performance benefit. Early results indicated this approach could achieve a maximum COP performance benefit on the order of 30%, while detailed analysis showed a COP performance benefit of 20% after inclusion of the air-side components in the model and accounting for fan power. However, significant system architecture changes are required with additional components, increased unit size, and increased cost.

- Desiccant-assisted air conditioners offer a solution which meets humidity and temperature requirements via decoupling latent and sensible loads. A solid desiccant wheel (DW) with Ferroaluminophosphate Zeolite was proposed to act

as a dehumidifier, allowing the vapor compression system to manage cooling function with a higher temperature evaporator. However, increased air flow rate was required to avoid condensation in the evaporator, resulting in higher evaporator fan power which reduced the system COP. At a high ambient temperature (43°C), the DW increased the sensible heat load, also leading to increased compressor power. While the DW technology has the capability to achieve the desired SSLC effect, it does not come without performance penalties, as well as added system cost, and challenges with integration into a split AC system.

- A SSLC system can utilize two evaporators, one with higher temperature to provide sensible cooling at higher air-flow rates, and another with lower temperature to provide dehumidification. Applying this approach, a traditional vapor compression cycle with dual evaporators has higher expansion losses than a conventional configuration, which resulted in a 13.4% performance degradation in COP compared to the baseline.

- Alternative AHU HX configurations and designs are harmonious with the other potential concepts and play an important part of any next generation AHU design. Utilizing properly optimized single slab HX designs in place of an A-coil led to 44–49% reduction in aluminum, 47–60% less refrigerant charge, and improved HX velocity distribution. Natural refrigerants and improved HX velocity distribution offer additional performance gains on the order of 2-4%.

- An ejector employed as an expansion device can recover expansion losses, boost pressure, and facilitate an efficient dual evaporator system. Four categories of ejector enhanced vapor compression cycles were investigated, leading to seven potential system concepts, with required component or configuration changes targeted within the AHU alone. Condenser outlet split (COS) and diffuser outlet split (DOS) ejector enhanced cycles improved SEER by 4%–8% above the 15 SEER baseline system, and improved COP by 9%–11%.

- While the primary objectives of the Phase I project focused on the AHU alone, not on the outdoor unit, analysis was conducted for a high-level system concept for a variable capacity air conditioner (AC) enabled by electronically commutated motor (ECM) fans and a variable speed compressor. While single-speed systems are common throughout the United States, variable speed will become prevalent as energy efficiency standards demand better performance. Understanding the impacts of variable speed operation are critical to planning for future product

commercialization. Results indicated that a variable capacity system concept is synergetic with any of the AHU solutions proposed above, but detailed analysis was considered beyond the scope of Phase I effort.

As can be seen from the above list, DW and split evaporators on their own not only do not meet target goals, they resulted in degraded performance. Inclusion of an ejector, however, coupled with optimized HX design is a promising solution for both single- and variable-speed systems.

As such, the Phase I effort yielded a combined concept for a next generation AHU: an ejector enhanced vapor compression cycle (COS or DOS), and an alternative dual-circuited evaporator angled-slab HX configuration. The COS and DOS ejector enhanced cycles improved performance above the 15 SEER baseline system by 4%–8%, and improved total COP by 9%–11%. With the COS or DOS ejector enhanced cycles, the AHU losses in the form of exergy destruction were reduced by up to 18%.

A properly optimized single slab HX design in place of the A-coil led to a 44–49% reduction in aluminum, a 47–60% less refrigerant charge, and improved HX flow distribution. The reduction of material and charge can offset costs from the addition of the ejector. Natural refrigerants and improved HX velocity distribution offer additional performance gains on the order of 2-4%.

Although the energy efficiency improvements described by the next generation AHU met the > 5% system target, with modifications limited to the AHU only, they did not approach the dual VCS SSLC benefit of 20%. There is opportunity to improve the ejector enhanced cycles by driving the low temperature evaporator further towards a latent HX, perhaps with a novel air-to-air HX. While not part of the scope of this project, system concepts that incorporate innovative heat exchanger designs and expand beyond the AHU, to the outdoor unit as well, offer possibilities to reach energy efficiency gains aspiring to the theoretical SSLC maximum benefit. Additionally, such systems offer opportunities in terms of novel intellectual property.

1. Identification and Significance of the Problem or Opportunity

Residential air handling units (AHUs) have essentially stayed the same in size, shape, form, and efficiency for the past 30+ years. While incremental improvements have been made to address safety, functionality, and energy-efficiency concerns, overall AHU structure has remained the same. Significant change is needed to develop a next generation design that can more readily address the increasing energy challenges of tomorrow. This includes reducing the contribution of HVAC systems on overall energy consumption, which accounted for a total of 9,114 trillion Btu, or 51% of the total energy for U.S. residential households in 2015 (U.S. EIA, 2018).

AHUs consist of a small number of typical components: an enclosure which forms the air flow path, a filter, a blower and motor, HX(s) with air flow baffles, condensate drain pan(s), refrigerant tubing, and a cooling mode refrigerant expansion device. An AHU can optionally contain an auxiliary electric resistance heater, or in the case of gas or oil-fired systems, a burner. Heating and cooling are typically delivered through a series of ducts throughout the home.

Losses in performance from the heating/cooling system, including the AHU itself, account for 70% or more; the remainder is lost due to duct leakage and often unaccounted additional pressure drop imposed on the blower (BTO, 2012). A next generation AHU must address the heating/cooling system losses. Typical losses for an air conditioning system are illustrated in Figure 1.

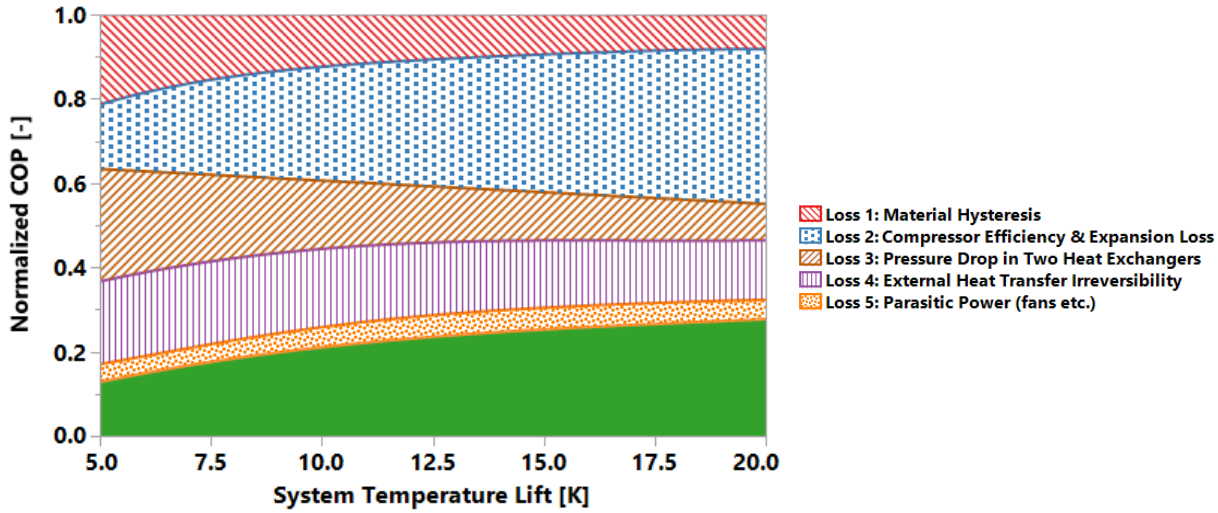

Figure 1: Typical losses in AC systems (Radermacher & Hwang, 2016).

Irreversibilities due to the compression process and finite temperature difference heat transfer in the HXs make the largest contributions to system-level performance reduction. In recent years, increasing demands to improve AC and heat pump efficiency have led manufacturers to improve condenser performance as a means of reducing system pressure lift and therefore energy consumption – as illustrated by the process 1-4 in the hypothetical T-s diagram in Figure 2.

Such improvements have been effective and are evident in an obvious increase in AC outdoor unit (ODU) size in residential systems over time. Improvements to indoor unit performance have not been so easy to achieve; the function of an AC indoor unit is not only to sensibly cool, but also to dehumidify a space, requiring an evaporating temperature below the incoming air dewpoint. If a more-effective evaporator were employed, approach temperature would be reduced, the compressor would consume less power, however the AHU would no longer adequately dehumidify the space (process 5-7 in the hypothetical T-s diagram in Figure 2).

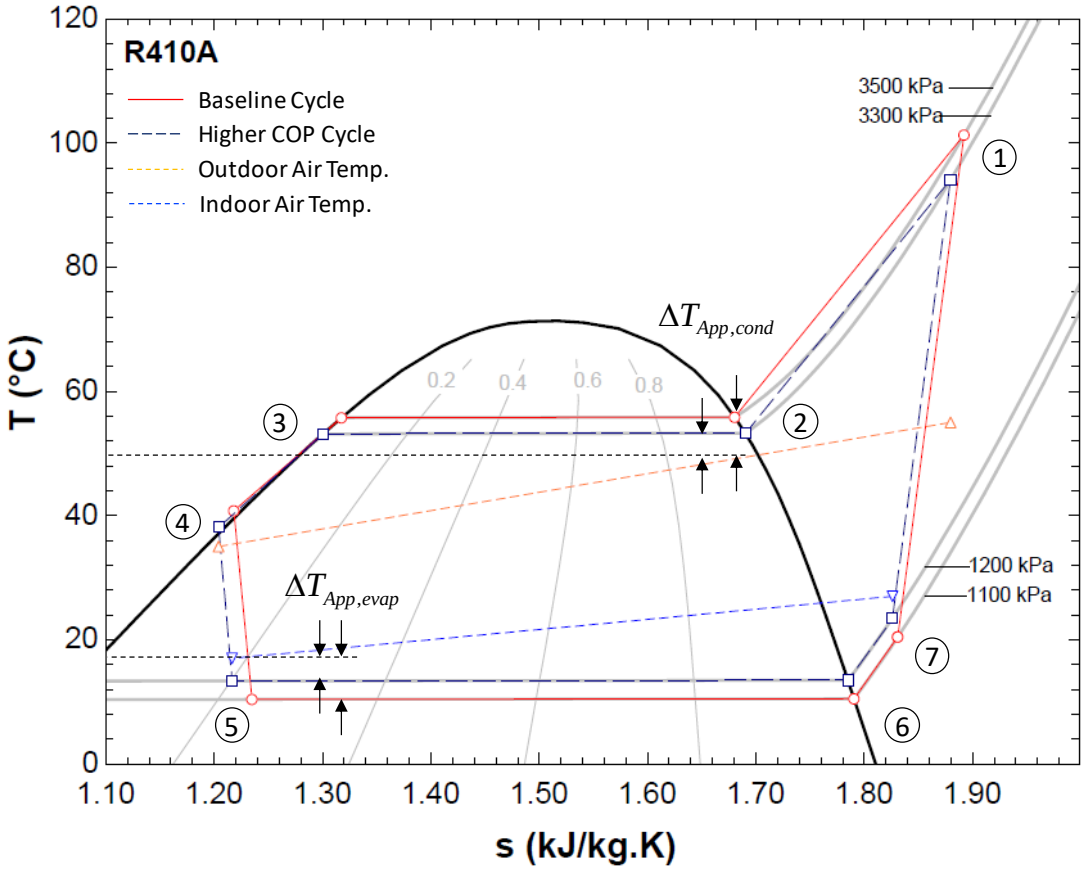

Figure 2: Hypothetical T-s diagram for R410A vapor compression cycles.

The primary energy-consuming components inside the air handler control volume are the blower and motor. The blower must overcome flow resistance from the HX as well as a building's ductwork. While variable speed fans and high efficiency motors have been able to reduce blower electricity consumption for single- and two-stage furnaces between 38–67% (Kendall, 2004), these technologies are already well understood and are often not implemented due high cost and lost efficiency improvements resulting from undersized ducting in the field (Yin and Pate, 2019). Parasitic power losses are a relatively small percentage of the overall losses in a system and other factors can contribute to greater overall system improvements.

In the case of the residential AHU, therefore, there is more performance improvement to be gained by focusing on improvements which can increase efficiency of the vapor compression cycle, rather than only on the blower or motor. To improve AHU and system performance, OTS focused on methods to reduce the approach temperature and pressure drop within the HX. An integrated approach for the full AHU requires improvement not only in the HX design, but also in establishing proper air distribution and improving dehumidification capability.

Dehumidification is a key function of the AHU, but it limits the cycles efficiency by requiring low evaporating temperatures. Numerous authors have evaluated the potential of separate sensible and latent cooling (SSLC), where the sensible cooling process can be performed at a higher temperature and efficiency, while latent cooling (dehumidification) is performed by a separate process. The separation of these processes can lead to systems with as much as 22-50% energy savings (Ling, 2011). Furthermore, AHUs installed in new buildings have an increasing demand to condition outside ventilation air in addition to the return air. Tighter envelope construction has resulted in an increased need for mechanical ventilation to satisfy indoor air quality requirements. Outside air is typically introduced via a single duct connected to the exterior of the building with simple damper control. In many installations, this outside air is introduced without conditioning or energy recovery, requiring the AHU to condition the air mixed with the building return air. This increases the potential for increased humidity levels and overall energy consumption.

By identifying new and effective methods of exchanging heat within the AHU and providing conditioned air for the home, a next generation design can be developed to deliver improved thermal comfort, adequate ventilation, and reduced energy consumption.

2. Technical Objectives

Project objectives set forth in the FOA for Topic 9a: Next Generation Residential Air Handlers, DE-FOA-0001941 are shown in Table 1.

Table 1: Next Generation Residential AHU Targets

Target Type	Target Description / Value
Heating and/or Cooling Mode Energy Efficiency	> 25% decrease in the energy consumption of an air handler or AHU and enhance the overall energy efficiency performance of the HVAC system > 5%
Physical Size	< 10% greater than state-of-the-art designs
Required cleaning intervals (or difficulty of cleaning) to maintain as-new performance	Little to no increase as compared to state-of-the-art designs, should improve system reliability
Susceptibility to damage or corrosion or performance degradation during manufacture, assembly, transportation, installation, or use.	Little to no increase as compared to state-of-the-art designs for relevant applications
System First Cost	No increase as compared to state-of-the-art system designs

3. Technical Approach

In this project OTS first focused on improving technical understanding of the function and form of the AHU. The key functions of the AHU are cooling and dehumidification of air. The AHU subsystems and components offer supporting functions of moving and guiding air, transferring heat, and removing moisture. OTS established a baseline using a commercially available AHU and modeled its components and systems. Computational fluid dynamics (CFD) was employed to visualize and quantify the air flow through the AHU and to understand the velocity distribution at the HX.

With respect to improving AHU performance OTS focused on:

- Minimizing HX approach temperature
- Identifying opportunities to reduce air maldistribution

- Development of multiple alternative system configurations which can more efficiently handle sensible and latent loads.

A hypothetical dual vapor compression system SSLC concept was studied to inform work on alternative concepts and to show the best-case theoretical performance benefit.

For the AHU system and components, OTS developed and evaluated multiple concepts in several solution categories:

1. Ejector enhanced vapor compression cycles
    a. Standard two-phase ejector
    b. Condenser outlet split (COS), 2 variants
    c. Diffuser outlet split (DOS)
    d. Separator outlet split, 3 variants
2. Desiccant assisted dehumidification
    a. Solid desiccant wheel SSLC
3. Dual evaporator SSLC
    a. Dual evaporator traditional vapor compression cycle
    b. Dual evaporator alternative cycles (ejector-based 1b-1d)
4. Alternative AHU HX configurations
    a. A-coil and single slab configurations

Four categories (1a-1d) of ejector enhanced vapor compression cycles were investigated leading to seven potential system concepts. The required component or configuration changes for these systems would be implemented in the indoor unit (AHU).

Desiccant air conditioners offer a solution which meets humidity and temperature requirements via decoupling latent and sensible loads. A solid desiccant wheel (2a), formed with AQSOA™ Ferroaluminophosphate Zeolite, acts as a dehumidifier, allowing the vapor compression system to manage cooling function at higher evaporating temperature.

Another SSLC approach is to utilize two evaporators, one with higher temperature to provide sensible cooling, and another with lower temperature to provide dehumidification (3a-3b).

The fourth category, alternative AHU HX configuration, is harmonious with concepts 1-3 and plays an important part of any next generation AHU design.

The primary objectives of the Phase I project focused on the AHU, not the outdoor unit. However, OTS additionally framed a high-level system concept for a variable capacity AC enabled by ECM fans and a variable speed compressor. The intent for the system was sensing and matching system capacity to the required sensible and latent cooling loads. The variable capacity system concept is synergetic with any of the AHU solutions proposed above. However, further development was considered out of scope for Phase I, though it should be considered as a natural evolution when combined with the concepts above.

3.1. Baseline Air Handling Unit & System

3.1.1. Baseline System Overview

OTS selected the Goodman AVPTC AHU to represent the baseline design (Goodman, 2018). This unit can be installed in multiple positions, and includes a variable speed, ECM-based blower system. The AHU is compatible with multi-stage heat pump and cooling applications and includes an internal thermostatic expansion valve (TXV). The unit is a “draw through” configuration where air is drawn through the A-coil and the centrifugal blower is mounted toward to the discharge end of the unit.

The unit is available in capacities ranging between 1.5 and 5 tons and two cabinet sizes. Capacities for 56% of all air conditioners and heat pumps shipped nationwide in 2018 were between 22 and 38.9 kBtuh (1.8 – 3.3 tons), with the largest single category volume occurring in the 33 – 38 kBtuh range at 21% (AHRI, 2019). Based on this data the specific model selected as the baseline for this project was the Goodman AVPTC 37D14A residential AHU. The AHU was paired with an appropriate outdoor unit with nominal 15 SEER / 8.8 HSPF rating based on DOE energy standards to take effect in 2023 (EERE–2014–BT–STD–0048). The selected AHU has a capacity of 36 kBtuh (3 ton).

Figure 3 shows a simplified schematic of the baseline system comprised of typical components of a vapor compression cycle. The indoor unit (AHU) contains an air to refrigerant fin and tube HX which acts as the evaporator in cooling mode, an expansion valve, and a centrifugal blower. The outdoor unit consists of an air to refrigerant fin and tube HX which acts as the condenser in cooling mode, a compressor, and a fan. Refrigerant tubing is shown in green and the air flow path in

orange. The state points 1-4 are indicated on the left in the schematic and shown on the right on the P-h diagram for the R410A refrigerant.

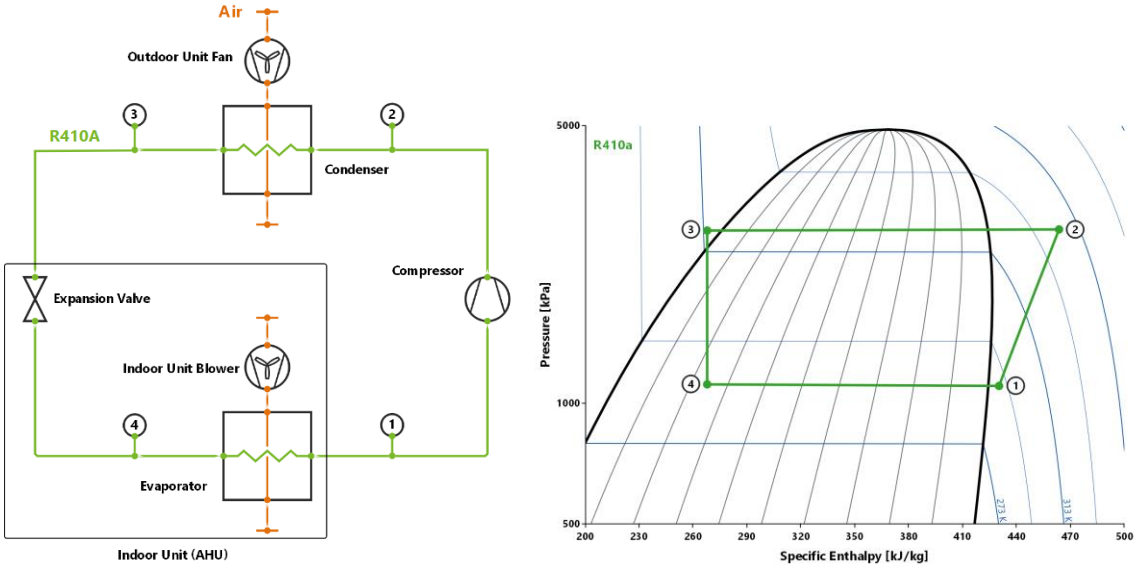

Figure 3: Baseline system – left: simplified schematic, right: P-h diagram.

3.1.2. Baseline Models of Heat Exchangers & Vapor Compression System

With the assistance of Goodman, baseline modeling included system-level and AHU-level modeling with the proprietary software tools CoilDesigner® and VapCyc®, as well as CFD simulations. CoilDesigner® was used to model each of the HXs: the A-Coil in the AHU (indoor unit), and the HX in the outdoor unit. VapCyc® was used initially to model the baseline vapor compression system. The VapCyc® model made use of the CoilDesigner® HX models as well as a 10-coefficient compressor model with coefficients provided by the compressor manufacturer.

Since alternative vapor compression cycles and other technologies were considered which were outside the typical capabilities of VapCyc®, two types of baseline models were implemented in Engineering Equation Solver (EES). The first type of model was a simplified model of the refrigerant side of the vapor compression cycle with no air side details. Simplified models were used primarily for comparison and screening of system topology concepts. The second type of model was more detailed and included the air side of the HXs. Detailed models formed the basis for comparison of baseline system performance to alternative vapor compression cycles and other technologies.

Relevant assumptions for the simplified and detailed models will be covered later in this report.

3.1.3. Air Flow Maldistribution

To maximize HX face area AHUs typically employ an A-coil formed from two HX slabs arranged in the form of a capital letter A. The HX slabs are mounted together with brackets and an airflow deflector is used at the apex of the A-coil to guide the air and potentially the condensate depending on unit orientation. Drain pans are arranged to collect condensate shed from the evaporator during cooling. If the AHU is multi-position it will have more than one arrangement of drain pans to support installation in vertical and horizontal orientations. Refrigerant tubing, especially the header, form additional obstruction and interference with the air flow. A photo of an A-coil and some of the components inside the AHU are shown in Figure 4. Drain pans (gray plastic components) can be seen at the bottom of the image and at the upper left. The refrigerant header can be seen at the upper right.

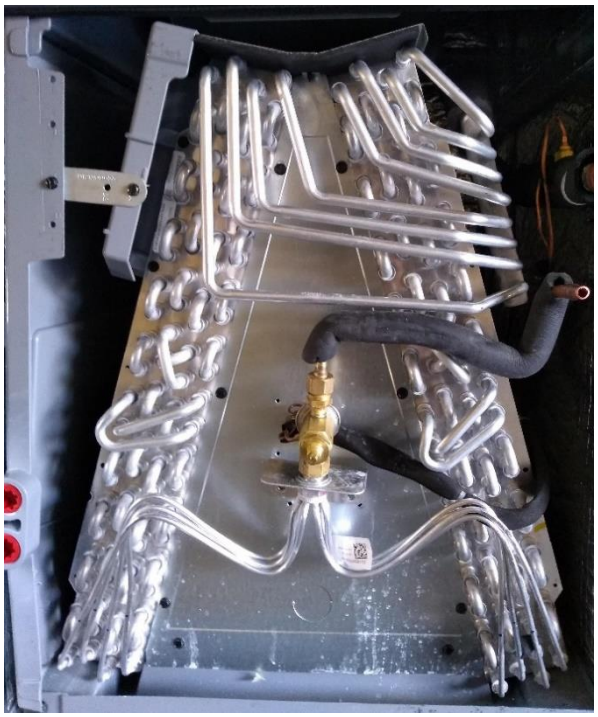

Figure 4: Photo of an A-Coil inside the AHU.

Numerous researchers have utilized experimental particle image velocimetry (PIV) and/or CFD to quantify air flow maldistribution, and testing or models to gauge the impact on HX and system performance. See Yashar & Cho (2007), Yashar & Domanski (2009), Li et al. (2018), A representative plot of a general normalized velocity distribution along the surface of a single slab of an A-coil, provided by Goodman, is shown in Figure 5. Air flow velocities are zero at the upstream end of the A-coil slab,

reach a maximum midway along the coil, and decrease again towards the downstream end of the slab near the air flow deflector.

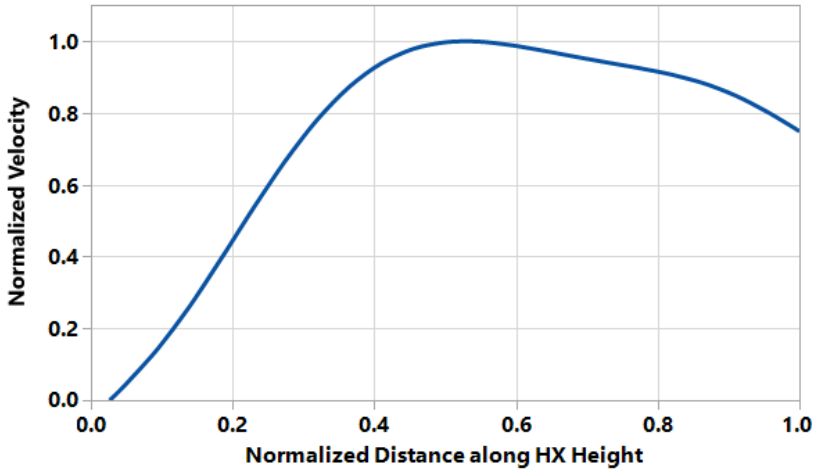

Figure 5: Representative velocity profile of a single A-coil slab.

Impact of the provided non-uniform velocity distribution on the A-coil HX slab performance was assessed via simulation with CoilDesigner®, and impact on system level performance via simulation with VapCyc®. Results from an A-coil slab with the velocity profile shown in Figure 5 revealed that the total cooling capacity was reduced by 3.4% compared to baseline with a uniform velocity distribution. The sensible capacity of the A-coil slab was reduced by 1.7% and the latent capacity was reduced by 8.8%. System level simulation showed a 1.9% reduction in total cooling capacity and COP compared to the baseline case with uniform velocity distribution.

CFD simulations were performed to assess the general behavior of the air flow in the AHU and to determine the velocity distribution along the A-coil surface for the baseline AHU. The CFD computational domain is the three-dimensional fluid volume of the AHU with A-coil slabs, shown in Figure 6. The domain includes porous zones to model the left and right coil slabs and a moving reference frame to model the blower rotation. The blower was set to rotate at a constant 800 rpm. Fluid (air) properties were set to constant density and viscosity, and turbulence was evaluated using a k-ε realizable model with enhanced wall treatment. The CFD geometry was meshed in ANSYS Fluent with a poly-hexcore mesh with relatively fine cells near the fluid region walls and growing layers with a ratio of 1.2. The generated mesh consisted of 1.15M cells.

A view of velocity vectors in the AHU air flow path are shown in Figure 7 and a plot of the normalized velocity distribution derived from CFD is shown in Figure 8.

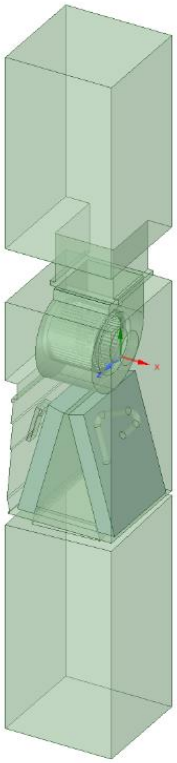

Figure 6: Computational domain of the AHU.

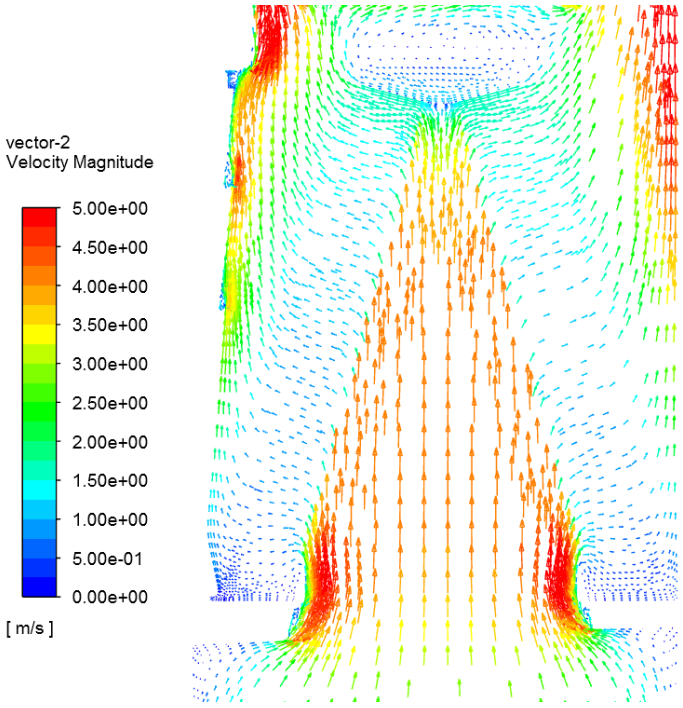

Figure 7: Velocity Vectors in cross-section of the AHU Near the A-coil.

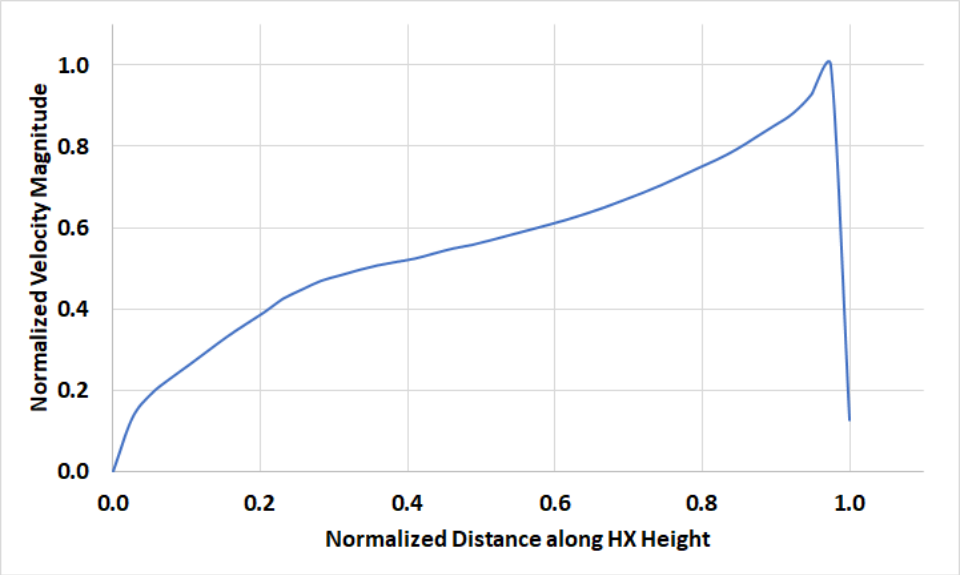

Figure 8: Velocity profile at outlet of a single A-coil slab.

Figure 7 shows relatively high air velocities near the A-coil inlet, especially where the obtrusive drain pan narrows the air flow path. The area directly above the A-coil airflow deflector shows near-zero velocity magnitudes. As shown in Figure 8, the velocity profile at the outlet of the left-hand side coil shows zero velocity at the bottom edge of the coil (distance = 0), gradually increasing to its maximum near the upper edge of the coil before slowing at the airflow deflector. In comparison, an ideal airflow distribution would have a constant velocity magnitude across the entire height of the HX. Without compensation, airflow maldistribution as shown in Figure 8 will degrade overall capacity and COP.

3.1.4. Simplified Vapor Compression System Modeling

The simplified VCS model incorporated the following assumptions:

- Fixed evaporator capacity
- Fixed evaporation temperature
- Fixed condensing temperature
- Prescribed compressor mass flow & isentropic efficiency
- Prescribed superheat & subcooling temperatures.

The values for these fixed or prescribed parameters were derived from system model runs completed in VapCyc® and are shown in Table 2.

Table 2: Simplified Model Parameters.

Parameter	Variable	Value
Evaporator Capacity [kW]	$\dot{Q}_{evap}$	10.55
Evaporation Temperature [°C]	T_{evap}	10.42
Condensing Temperature [°C]	T_{cond}	37.95
Superheat Temperature [°C]	ΔT_{SH}	5.0
Subcooling Temperature [°C]	ΔT_{SC}	4.0
Refrigerant Mass Flow Rate [g/s]	$\dot{m}_{comp}$	63.92
Compressor Isentropic Efficiency [-]	η_{comp}	0.733

The simplified baseline system model with these parameters was found to have a COP of 6.27. This COP was calculated using the compressor power. Power from fans was not included as the air side of the system was not modeled.

3.1.5. Second Law Analysis of Baseline System

Thermodynamic analyses are primarily based on the First Law of Thermodynamics. Kotas (1985) lists two typical steps in traditional thermodynamic analysis:

1) "Use of an energy balance on the system, usually to determine 'unaccounted for' heat transfer between a system and its environment".
2) "Calculation of a criterion of performance relevant to the system under consideration."

In addition to the traditional thermodynamic analysis of energy balances and calculation of performance criteria, a Second Law Analysis was performed on the baseline and each candidate system using exergy balances. This allows a component by component accounting of losses due to irreversibilities.

Exergy is a measure of the availability or 'usability' of energy and irreversibility is the loss of exergy. Klein and Nellis (2012) define exergy as the "capability to do useful work using thermodynamically perfect (ie. reversible) processes". Exergy is a relative metric and is defined with reference to 'dead' state which is in thermodynamic equilibrium. The environmental state used as a reference was: $T_o = 25\ °C$ and $P_o = 101.325\ kPa$. The enthalpy at this state is represented by h_o, and entropy by s_o.

Specific exergy is defined in Equation (1), and exergy destruction by Equation (2):

$$\phi = h - h_o - T_o \cdot (s - s_o) \tag{1}$$

$$\dot{\phi}_{\text{dest}} = \dot{Q}\left(1 - \frac{T_o}{T}\right) - \dot{W} + \sum \dot{m}_{in}\,\phi_{in} - \sum \dot{m}_{out}\,\phi_{out} \tag{2}$$

where, in this application, $\dot{Q}$ is capacity, $\dot{W}$ is work input, and $\dot{m}$ is mass flow rate.

A Sankey diagram typically depicts the flow of energy where flows can branch but the overall width of the flows is constant as energy is conserved. While similar to a Sankey diagram, a Grassman diagram depicts the total amount of work that can be extracted from a system. The amount of work available to be extracted decreases at each stage of a process.

The flow of destroyed exergy for the baseline system, derived from the simple model in cooling and using Equations (1) and (2), is shown in a Grassmann diagram in Figure 9. This approach was used to better understand the baseline system performance and to produce comparisons between the baseline and proposed alternative systems. Each component in the simplified baseline system was responsible for a portion of the total exergy destruction ranging from 10% for the expansion valve to 26.8% in the condenser.

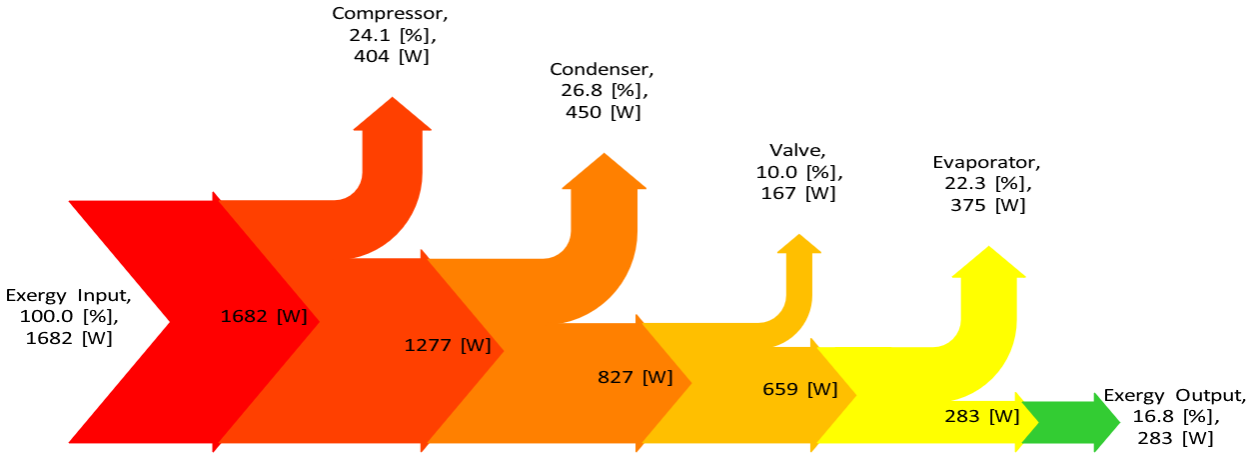

Figure 9: Grassmann diagram of the baseline vapor compression system.

For reference, the five types of losses discussed previously in Section 1, Figure 1 were:

1) Material hysteresis (refrigerant)
2) Compressor efficiency and expansion loss
3) Pressure drop in two HXs
4) External heat transfer irreversibility
5) Parasitic power (fan, etc.).

Loss types 3 and 5 were not considered in the simplified model.

The compressor and expansion valve (loss type 2) accounted for 34.1% of the exergy destroyed, while the HXs accounted for 49.1%. The remaining 16.8% represents the exergy efficiency of the baseline system, which can be described by Equation (3).

$$\eta_{ex} = 1 - \frac{\dot{\phi}_{dest}}{\dot{W}_{comp}} \quad (3)$$

The total power input from the compressor was 1682 W and 283 W was used by the system. Components within the AHU, namely the evaporator and the expansion valve, accounted for 32.3% of the exergy destruction. The compressor and condenser from the outdoor unit accounted for 54.9%.

3.1.6. Detailed Vapor Compression System Modeling

Detailed system models were developed in EES of the refrigerant & air sides of each vapor compression system considered.

For the baseline HXs, CoilDesigner® and VapCyc® were employed to conduct parametric runs over a range of expected conditions in order to develop regression model correlations of the product of the total heat transfer coefficient and area (UA_h) for both the indoor and outdoor unit coils. In the cooling case, where the indoor coil is acting as an evaporator, the product of the total mass transfer coefficient and area (UA_m) were found from parametric runs and regression models developed. Correlations which could represent the behavior of the HXs in the EES models were developed for each slab of the A-coil, the complete A-coil, and the outdoor unit HX.

A log-mean temperature (LMTD) & log mean humidity ratio (LMWD) approach was employed using the regression-based UA value correlations to calculate sensible and latent capacities.

A 10-coefficient compressor model including density, superheat, and power corrections was implemented. Compressor coefficients used were provided by the compressor manufacturer. Isentropic and volumetric efficiencies obtained from the base model were used as prescribed compressor efficiencies in other models.

The detailed system model had the following inputs:

- Indoor & outdoor unit inlet air temperatures & humidities.
- Indoor & outdoor unit air flow rates and fan powers.
- Compressor displacement, speed, & efficiencies.
- HX UA value correlation coefficients.
- Superheat & subcooling temperatures.
- Refrigerant side pressure losses.

Comparison of results from the detailed system model of the baseline was validated against results from VapCyc® (Table 3) at 35°C ambient temperature with good agreement found.

Table 3: VapCyc® and EES model comparison.

Parameter	Variable	VapCyc®	EES	Difference
Evaporator Air Outlet Temperature [°C]	$T_{a,evap,out}$	14.34	13.55	-0.79K
Evaporator Refrigerant Outlet Temperature [°C]	$T_{evap,out}$	16.68	15.80	-0.88K
Evaporator Capacity [kW]	$\dot{Q}_{evap}$	10.814	10.532	-2.60%
Evaporator Condensate Flow Rate [g/s]	$\dot{m}_{condensate}$	0.781	0.767	-1.78%
Condenser Air Outlet Temperature [°C]	$T_{a,cond,out}$	41.04	40.81	-0.23K
Condenser Refrigerant Outlet Temperature [°C]	$T_{cond,out}$	41.14	40.94	-0.20K
Condenser Capacity [kW]	$\dot{Q}_{cond}$	12.975	12.691	-2.19%
Compressor Power [kW]	$\dot{W}_{comp}$	2.162	2.160	-0.11%
Compressor COP [-]	COP_{comp}	5.00	4.88	-2.50%
Total COP [-]	COP_{total}	4.07	3.97	-2.57%

3.2. Hypothetical Dual Vapor Compression System Concept

3.2.1. Simplified Dual Vapor Compression System Modeling

To evaluate maximum potential efficiency gains from a SSLC approach, a hypothetical dual vapor compression system (VCS) was proposed using two independent vapor-compression cycles. One VCS would be designed to perform at a high evaporating temperature targeting the sensible heat load, and the other VCS would be designed with a high evaporator approach temperature targeting the latent load. The sensible subsystem with reduced approach temperature would improve overall efficiency of the combined system through reduction of compressor power and improved COP above the baseline performance.

A schematic diagram for the hypothetical dual VCS is shown in Figure 10 (left), along with a corresponding P-h diagram (right). The 'sensible' subsystem is the upper VCS in the schematic and the 'latent' subsystem is the lower VCS. The P-h diagram shows the sensible cycle in dark green (points 1-4) and the latent cycle in light green (points 5-8).

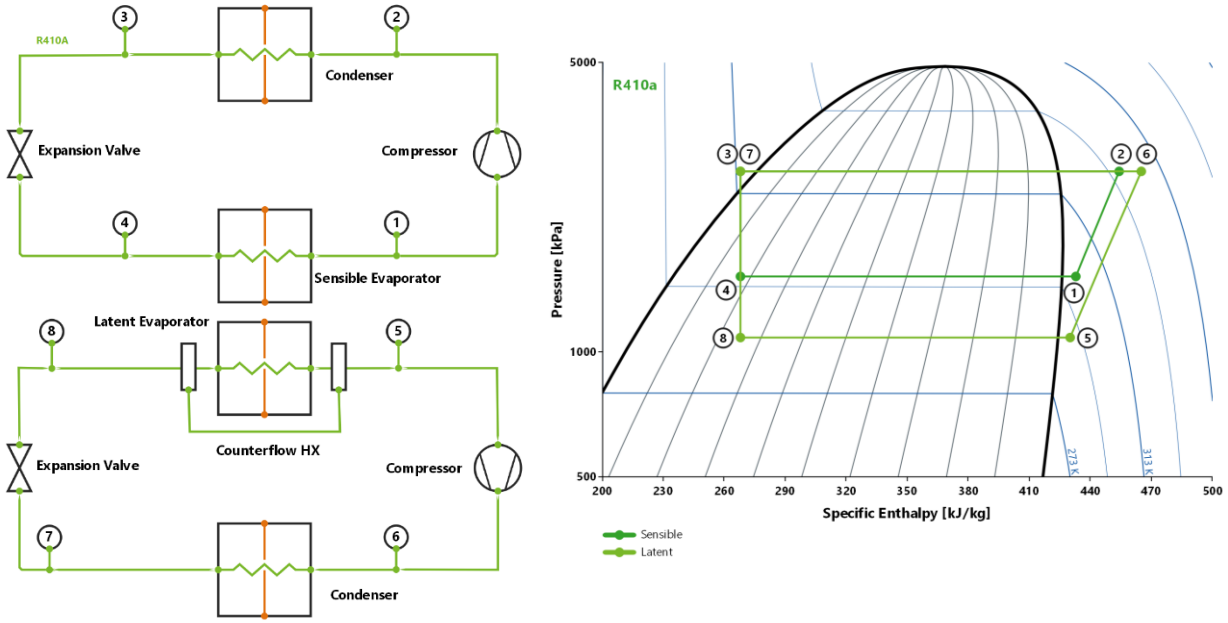

Figure 10: Dual VCS with SSLC– left: schematic, right: P-h diagram

In the schematic, a conceptual air-to-air counterflow HX is shown in the latent VCS arranged around the latent evaporator. The purpose of this component is to provide sensible precooling of the incoming air, increasing the relative humidity, such that the latent evaporator can primarily perform latent dehumidification.

An EES model was developed to compare the SSLC dual VCS against the baseline system. The subsystems were both assumed to meet a given sensible and latent load. The refrigerant used was R410A. The inlet air temperature was 27°C and the inlet relative humidity was 50%. The mass flow rate of the evaporator air was 0.30 kg/s. The outdoor air temperature was 35°C.

The total capacity assumption was 10.5 kW and the sensible heat ratio of the system was 0.75. The isentropic efficiency of the compressor was assumed to be 0.733 for all systems. The approach temperatures of the HXs were fixed for all systems. The baseline system assumed a fixed approach temperature of 15 K for the evaporator, and 10 K for the condenser. This gave the baseline system a condensing temperature of 45°C and an evaporating temperature of 12°C. The superheat and subcooling of the systems were also fixed. For all systems, the superheat was assumed to be 4°C, and the subcooling amount was assumed to be 5°C. Each condenser was assumed to have an approach temperature of 10 K.

The sensible subsystem was assumed to remove only sensible heat load. The sensible evaporator was assumed to have an approach temperature of 5 K. This raised the evaporation temperature to 22°C, which was above the dew point temperature of the inlet air (15.7°C), removing the possibility of dehumidification.

The latent subsystem was assumed to have a sensible heat ratio of 0.10. Most of the heat removed was latent heat, however, a small amount of sensible cooling was also assumed to occur. The total sensible and total latent capacity of the combined subsystems were assumed to match the sensible and latent capacity of the baseline system. Table 4 shows a comparison of baseline and dual VCS model performance.

Table 4: Comparison of baseline & dual VCS performance.

Parameter	Baseline	Dual System	Increase over Baseline
COP	4.99	6.51	30%
Sensible Capacity [kW]	7.875	7.875	0%
Latent Capacity [kW]	2.625	2.625	0%
Work [kW]	2.103	1.612	-23%
Mass Flow Rate [kg/s]	0.065	0.064	-1%

The dual VCS design showed a significant efficiency improvement with a COP increase over baseline of 30%. The reduction in pressure lift in the sensible system

allowed the compressor to operate more efficiently, allowing the dual system to reduce compressor work overall, making up for the increase in pressure lift in the latent system. Table 5 shows a comparison of the performance of the sensible and latent system performance and conditions. The goal of this effort was to understand the potential benefits of targeting sensible and latent cooling directly, instead of handling both with a single system having an evaporation temperature below the dew point.

Table 5: Comparison of baseline & dual system model performance.

Parameter	Sensible System	Latent System
COP	7.71	4.64
Sensible Capacity [kW]	7.58	0.29
Latent Capacity [kW]	0	2.63
Work [kW]	0.983	0.629
Mass Flow Rate [kg/s]	0.046	0.018
Evaporation Temp. [°C]	22	10

Such a system could be achieved using two dedicated evaporators; the sensible evaporator would need to be larger than the latent evaporator to reduce the approach temperature and increase the evaporating temperature as much as possible. To maximize efficiency, ideally, both systems would not be run at the simultaneously. The latent-dedicated evaporator would only be used when latent cooling was needed.

3.2.2. Detailed Dual Vapor Compression System Modeling

A dual VCS would require significant system architecture changes impacting both the AHU and the ODU. Consequently, this concept was considered out of scope based on the AHU specific focus of this project. However, further analysis was conducted to inform work on other SSLC concepts, as well as to provide a practical view of the potential efficiency improvement compared to the theoretical 30% COP increase.

The dual VCS was modeled in EES as two subsystems: a sensible subsystem, and a latent subsystem. The subsystem models were connected by boundary conditions, with the sensible evaporator outlet air state taken as an input to the inlet air state of the latent system counterflow heat exchanger.

The sensible subsystem model had the following inputs and assumptions:

- 7.331 kW fixed capacity at 28°C outdoor temperature.
- Fixed condensing temperature 39°C.
- Fixed evaporating temperature 18°C.
- Fixed condenser airflow rate at 60% of baseline.
- Fixed air outlet temperature 20°C.

The latent subsystem model had the following inputs and assumptions:

- 2.683 kW fixed capacity at 28°C outdoor temperature.
- Fixed sensible heat ratio of 0.3.
- Fixed condensing temperature 39°C.
- Fixed evaporating temperature 10°C.
- Fixed condenser airflow rate at 40% of baseline.
- Fixed evaporator airflow rate at 100% of baseline.
- Evaporator face area receives a portion of sensible evaporator air flow.

A factor was used to scale compressor mass flow rates and power from the 10 coefficient compressor maps. EES models were solved to meet the given constraints yielding the evaporator, condenser, and counterflow HX sizes; as well as the compressor sizes. The dual VCS system parameters are summarized in Table 6.

Results showed that in the dual VCS configuration both compressors could be reduced in size relative to baseline, leading to a total compressor size reduction of 14% overall. The sensible system compressor size was reduced to 51.4% of baseline and the latent system compressor was reduced in size to 34.8% of baseline.

Overall condenser UA was 2% less than baseline. The sensible system condenser UA was 0.599 kW/K and the latent condenser UA was 0.287 kW/K.

For the sensible system evaporator to perform solely sensible cooling, the UA and air flow rate were both required to increase significantly. The sensible system evaporator UA was increased by 43% and the air volume flow rate by 71% relative to baseline, while the latent system evaporator was 35% smaller, and the total evaporator UA increase was 107% of baseline.

Table 6: Dual VCS system configuration compared to baseline.

Parameter	Baseline	Sensible Subsystem	Latent Subsystem	Combined Dual VCS	Dual VCS vs. Baseline
Compressor size ratio [-]	1	0.514	0.348	0.862	-14%
Condenser UA [kW/K]	0.9	0.599	0.287	0.885	-2%
Evaporator UA [kW/K]	1.8	2.57	1.17	3.73	107%
Evaporator air volume flow rate [m^3/s]	0.516	0.883	0.516	0.883	71%
Condenser air volume flow rate [m^3/s]	1.89	1.13	0.755	1.89	0%
Counterflow HX UA [kW/K]	0	—	1.06	—	—

The counterflow HX was used to increase the relative humidity of the air entering the latent system evaporator, decreasing the sensible heat ratio (SHR) and improving the latent system COP. A suitable UA value for the counterflow HX was determined to be 1.06 kW/K yielding a capacity of 1.92 kW. The temperature of the incoming air to the latent evaporator was reduced from 20°C to 17°C and the relative humidity was increased from 76.3% to 92.3%.

A summary of the operating characteristics of the dual VCS is shown in Table 7. With an increased evaporating temperature of 18°C, and an SHR of 1, the sensible subsystem compressor COP improved to 8.10 compared to the baseline of 6.07. The latent subsystem evaporating temperature was 10°C, with the targeted SHR of 0.3, giving a compressor COP of 5.89 compared to the baseline of 6.07. These results show that system energy efficiency benefit could be maximized by preferentially operating the sensible subsystem and only operating the latent subsystem as required.

Results for total COP for the baseline and dual VCS are shown in Table 8. The dual VCS combined system total COP was found to improve 20% to 5.76 compared to the baseline COP of 4.80.

Table 7: Operating characteristics of the Dual VCS.

Parameter	Sensible Subsystem	Latent Subsystem
COP [-]	8.10	5.89
Compressor power [kW]	0.905	0.651
Total evaporator capacity [kW]	7.33	3.83
Latent evaporator capacity [kW]	0	2.68
SHR [-]	1	0.3
Condensing temperature [°C]	39	39
Evaporating temperature [°C]	18	10
Counterflow HX capacity [kW]	—	1.92

Table 8: Comparison of baseline & dual VCS COP total.

Parameter	Baseline	Dual System	Increase over Baseline
Total COP	4.80	5.76	20%

Improvements possible from a SSLC dual VCS were promising though several practical considerations should be reviewed related to the design and required system architecture changes. The dual VCS design detailed here would result in an increase in overall AHU size and would not meet the DOE requested physical size target due to the required increase in evaporator size for the sensible subsystem. Also, the changes required would impact both the AHU and the ODU. The counterflow HX design would need to be compact and would require an innovative solution for integration into the AHU. System cost would increase based on the increased number of required components even though some of those components would be smaller in size than the baseline.

In summary, based on the detailed analysis the dual VCS was found to approach the ideal savings potential, but with additional hardware, system cost, and system size. The internal counterflow air-to-air HX was a key contributor to the performance of the latent only subsystem and potential novel intellectual property could be developed by integrating the evaporators and the counterflow HX into a single coil.

Alternatively, SSLC concepts could be implemented in a single VCS in several ways: a single-speed compressor system with time-based switching between operating modes, a system using two dedicated evaporators, a two-stage system, or a system with a variable speed compressor and fans. The variable speed compressor and fans will be discussed further in Section 3.6.

3.3. Dual Evaporator System Concept

A dual evaporator air-conditioning system could form the basis of one type of SSLC technology. A first evaporator would operate at a higher evaporating temperature and handle sensible cooling. A second evaporator would operate at a lower evaporating temperature and handle the latent load (dehumidification). Such a system is shown in Figure 11 (left) along with a corresponding P-h diagram (right). In addition to two evaporators, the system requires two expansion valves to reduce pressure from state 3 to states 4 and 6. Also needed is a metering valve to reduce the pressure of the refrigerant leaving the high temperature evaporator at state 5 to match the pressure at the outlet of the low temperature evaporator at state 1.

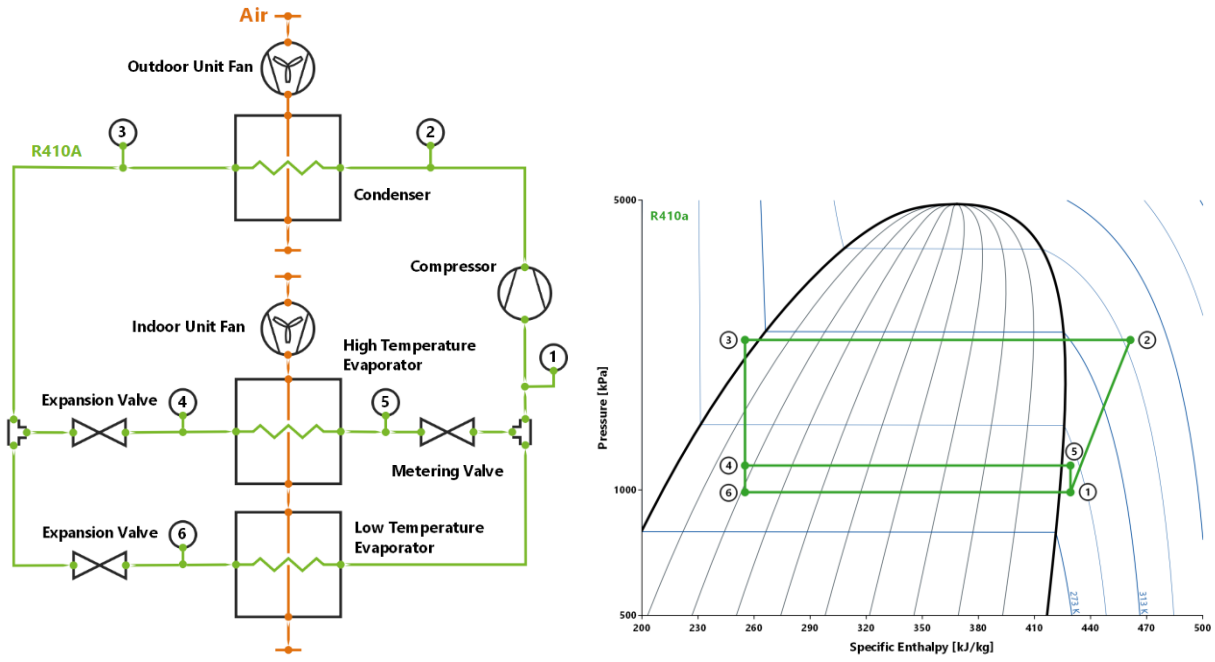

Figure 11: Dual evaporator system – left: schematic, right: P-h diagram

The dual evaporator system performance was evaluated with a basic vapor compression system model. Settings for key parameters are given in Table 9. The condensing temperature, superheat and subcooling temperatures, compressor efficiency, and refrigerant mass flow rate were taken to be the same as the baseline case.

Table 9: Parameters for the dual evaporator system.

Parameter	Variable	Value
Total Evaporator Capacity [kW]	$\dot{Q}_{evap}$	10.553
Evaporator capacity split [-]	y	0.65
Evaporator Capacity (high) [kW]	$\dot{Q}_{evap-high} = y \cdot \dot{Q}_{evap}$	6.86
Evaporator Capacity (low) [kW]	$\dot{Q}_{evap-low} = (1-y) \cdot \dot{Q}_{evap}$	3.70
Evaporation Temperature (high) [°C]	$T_{evap-high}$	12.0
Evaporation Temperature (low) [°C]	$T_{evap-low}$	7.0

The ratio of the refrigerant mass flows through the evaporators, μ_{evap}, is given by Equation (4):

$$\mu_{evap} = \frac{\dot{m}_{low}}{\dot{m}_{high}} \tag{4}$$

With an evaporator capacity split of 0.65 the flow ratio was 0.5385, obtained from the model. The mass flow averaged evaporation temperature was 10.25 °C compared to 10.45 °C for the baseline.

Performance results from the simplified model of the dual evaporator system are show in Table 10. The compressor power of the dual evaporator system was 261 W higher than the baseline, leading to a COP which was degraded by 13.4%. The exergy efficiency of the dual evaporator system was 10.2% lower than the baseline.

Table 10: Dual evaporator performance compared to baseline.

	Baseline	Dual Evaporator
Compressor Power [kW]	1.682	1.942
COP [-]	6.3	5.4
Exergy Efficiency [-]	16.9%	15.1%

The Grassmann diagram for the dual evaporator system is shown in Figure 12.

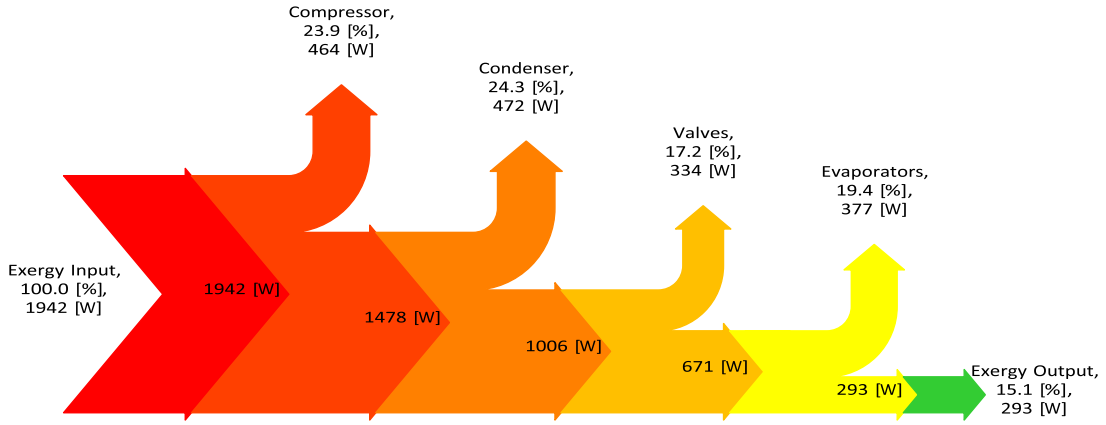

Figure 12: Grassmann diagram of dual evaporator vapor compression system.

With a 15.5% increased exergy input against baseline, from 261 W of additional compressor power, the exergy output yielded an increase of only 10 W, or 3.7% of the input. The combined exergy destruction from the valves accounted for 17.2% of the input. A comparison of the exergy destroyed by each component of the baseline and dual evaporator system is given in Table 11.

Table 11: Comparison of baseline & dual evaporator exergy destruction.

		Baseline	Dual Evaporator	Percent Increase over Baseline
Exergy Destroyed [W]	Compressor	405	465	14.8%
	Condenser	451	472	4.8%
	Valve(s)	168	335	99.6%
	Evaporator(s)	376	377	0.4%
	Total	1,399	1,649	17.9%

With the addition of a second expansion valve the losses due to expansion nearly doubled compared to the baseline. Any potential benefit from operating the high temperature evaporator at lower approach temperature was nullified by losses.

3.4. Ejector Enhanced Vapor Compression Cycles

3.4.1. Form and Function of an Ejector

In its simplest form, an ejector is a passive component with no moving parts. As shown in Figure 13 (ERTC, 2014), an ejector is essentially a pair of nozzles, which are usually co-annular, a mid-section which acts as a mixing chamber, and a diffuser.

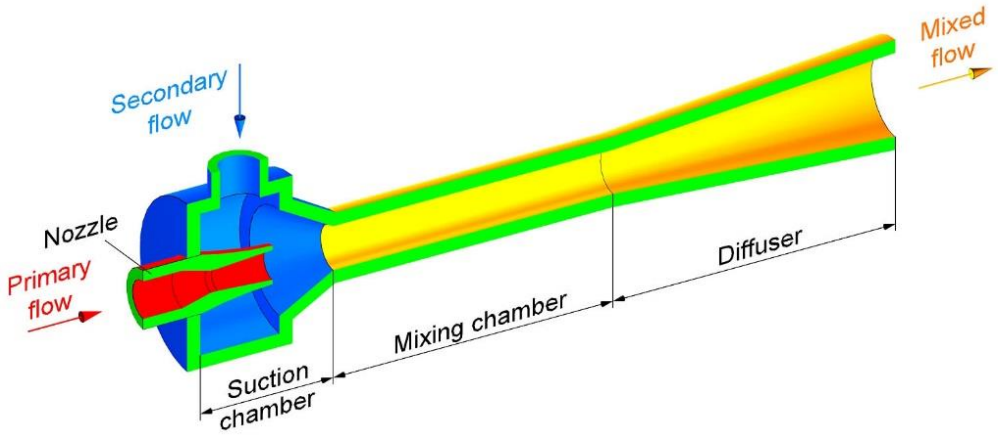

Figure 13: Cut-away view of an ejector.

The function of an ejector is two-fold: to entrain the flow of fluid, and to increase a fluid's pressure. A high-pressure fluid enters the motive nozzle, expands, and creates suction which entrains the flow of fluid into the secondary nozzle. The fluids then mix in the mixing chamber and exit through a diffuser. The diffuser compresses the fluid and increases the pressure of the exiting fluid mixture above the pressure level of the entrained secondary flow. In this way an ejector works as both an expansion device and a refrigerant pump. The objective of adding an ejector to a vapor compression cycle is to recover expansion losses and lift the pressure at the compressor suction so that the compressor can do less work. Therefore, the addition of an ejector to an AHU can address loss type 2, 'compressor efficiency and expansion loss', introduced in Section 1, Figure 1.

An ejector inherently merges two flow streams, and when used in conjunction with components which divide flows, such as tees or a liquid-vapor separator, various alternative vapor compression cycles and system configurations can be created depending on the placement of the ejector with respect to the other components. These configurations give rise to differences in the refrigerant states at the ejector. Configurations are possible which yield two-phase, superheated vapor, or saturated vapor states. Importantly, these system configurations also allow for introduction of

dual evaporator cycles with the potential to improve on the limitations of the dual evaporator cycle discussed in Section 3.3 and to potentially facilitate SSLC.

Following a discussion about the ejector modeling approach these alternate configurations are described in detail and evaluated using the simplified modeling approach.

3.4.2. Ejector Modeling Approach

An ejector model was integrated with both the simplified and detailed vapor compression system models described previously. The ejector model followed the approach from Kornhauser (1990).

Key assumptions in the ejector model were:

- Prescribed efficiencies were taken for each ejector nozzle & the diffuser.
- The suction pressure fraction of the ejector, n, was taken as a constant.
- The ejector mass flow ratio, r, was a constant.

The ejector motive nozzle, secondary nozzle, and diffuser efficiencies are defined as:

$$\eta_{mn} = \frac{h_{primary} - h_{mn}}{h_{primary} - h_{mn,s}} \tag{5}$$

$$\eta_{sn} = \frac{h_{secondary} - h_{sn}}{h_{secondary} - h_{sn,s}} \tag{6}$$

$$\eta_{diff} = \frac{h_{diff} - h_{mix}}{0.5 \cdot V_{mix}^2} \tag{7}$$

Values for the nozzle & diffuser efficiencies were those used by Lawrence and Elbel (2013): η_{mn}= 0.80 [-], η_{sn}= 0.80 [-], η_{diff}= 0.75 [-].

The suction pressure fraction of the ejector, n, relates the mixing pressure of the ejector to the pressure at the inlet of the secondary nozzle inlet pressure. This relationship is given in Equation (8):

$$P_{mix} = (1 - n) \cdot P_{secondary} \tag{8}$$

The diffuser exit flow is the sum of the motive and secondary nozzle flows:

$$\dot{m}_{diffuser} = \dot{m}_{motive} + \dot{m}_{secondary} \tag{9}$$

The ejector mass flow ratio is the ratio of the motive nozzle flow to the diffuser exit flow:

$$\mathrm{r} = \frac{\dot{m}_{motive}}{\dot{m}_{diffuser}} \tag{10}$$

Generally, the values of the parameters n and r were found by minimizing the sum of squares error in the energy balance. In the case of the two-phase ejector cycles, Kornhauser (1990) had previously shown that the diffuser exit quality is equal to the ejector mass flow ratio. Therefore, in the case of the two-phase ejector cycles, in addition to the energy balance error, the difference between the diffuser outlet quality and the ejector mass flow ratio was used in the objective function in a sum of squares minimization in order to match the diffuser exit vapor quality.

Ejector behavior can be described with the ejector pressure lift ratio, r_p, and the ejector entrainment ratio μ:

$$r_p = \frac{P_{diff}}{P_{secondary}} \tag{11}$$

$$\mu = \frac{\dot{m}_{motive}}{\dot{m}_{secondary}} \tag{12}$$

In addition to the relationships given above, the Kornhauser (1990) ejector model consists of the following equations:

$$V_{mn}^2 = 2 \cdot \left(h_{primary} - h_{mn}\right) \tag{13}$$

$$V_{sn}^2 = 2 \cdot \left(h_{secondary} - h_{sn}\right) \tag{14}$$

$$V_{mix} = r \cdot V_{mn} + (1 - r) \cdot V_{sn} \tag{15}$$

$$h_{mn,s} = f\left(refrigerant, P_{mix}, s_{primary}\right) \tag{16}$$

$$h_{sn,s} = f\left(\text{refrigerant}, P_{mix}, s_{secondary}\right) \tag{17}$$

$$h_{diff,s} = h_{mix} + 0.5 \cdot V_{mix}^2 \quad (18)$$

$$h_{diff} = (1 - r) \cdot h_{secondary} + r \cdot h_{primary} \quad (19)$$

$$P_{diff} = \mathrm{P}(\text{refrigerant}, h_{diff,s}, s_{mix}) \quad (20)$$

$$P_{mn} = P_{sn} = P_{mix} \quad (21)$$

$$s_{mix} = f(\text{refrigerant}, P_{mix}, h_{mix}) \quad (22)$$

Models for several vapor compression system configurations with ejectors were successfully validated against results from Lawrence and Elbel (2013) with good agreement found.

3.4.3. Ejector Enhanced Vapor Compression Cycle Concepts

Four categories of ejector enhanced vapor compression cycles were investigated leading to seven system concepts which were evaluated and screened using the simplified modeling approach. The four categories are named based on the refrigerant flow configuration referencing system components and are: the standard two-phase ejector cycle, the condenser outlet split (COS) cycle, the diffuser outlet split cycle (DOS), and the separator outlet split (SOS) cycle.

Shown in Figure 14, the standard two-phase ejector cycle employs a single evaporator and an ejector replaces the typical expansion valve in the system. The primary ejector flow is the high-pressure liquid leaving the condenser at point 3. The vapor at point 10, leaving the evaporator, is entrained by the secondary nozzle of the ejector. The ejector outlet flow at point 7 has a pressure which is higher than the evaporation pressure due to the ejector pressure lift. A liquid-vapor separator feeds vapor to the compressor and liquid to a metering valve. The metering valve further expands the refrigerant to the evaporator. Note that three of the points shown, in this case points 4-6, are internal states of the ejector and, while they are shown on the P-h diagram, the pressures at those internal points are static pressures. This will also be the case in the following discussion.

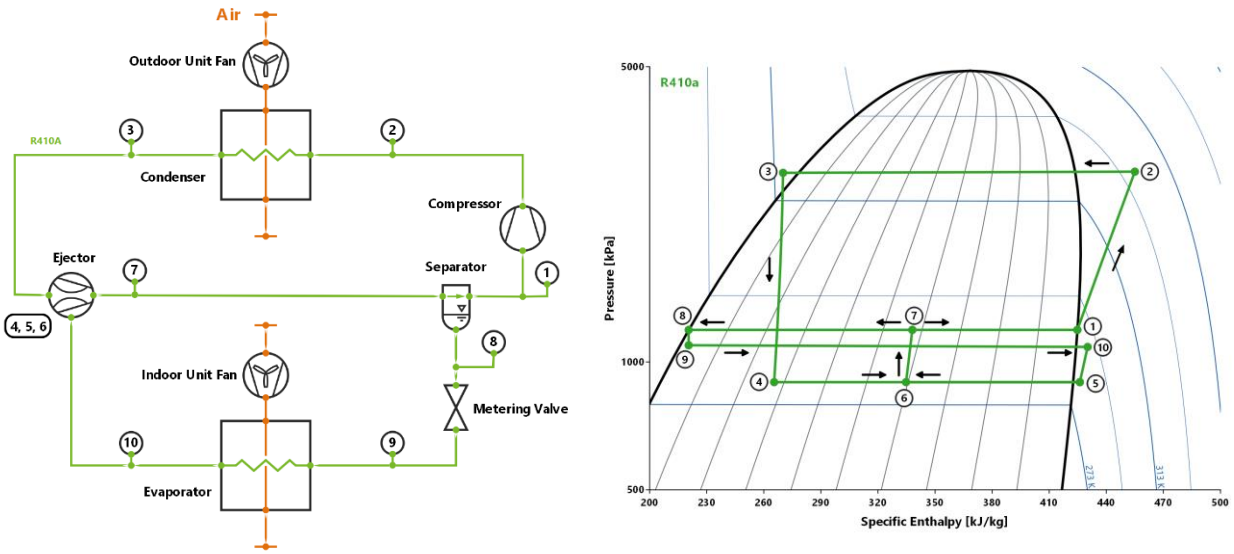

Figure 14: Standard two-phase ejector system – left: schematic, right: P-h diagram.

In contrast to the standard two-phase ejector cycle, the following six cycles, which are of types COS, DOS, or SOS systems; all utilize dual evaporators. In the case of these dual evaporator cycles the schematics show the air flow to the evaporators in series, with the high temperature evaporator receiving air flow first followed by the low temperature evaporator. Series air flow is not strictly necessary in these cycles. Parallel air flow to the evaporators may be desired in some applications.

Lawrence and Elbel (2013) detailed the two-phase condenser outlet split system (COS) shown in Figure 15. The name stems from the fact that the refrigerant flow splits after the condenser. In this system there are two evaporators in parallel in the refrigerant flow. An ejector is utilized as the expansion device for the high temperature evaporator and an expansion valve is employed for the low temperature evaporator. There is no liquid-vapor separator. The second evaporator operates at a lower temperature and has a lower refrigerant mass flow rate. The high temperature evaporator sees lifted pressure at point 7 and its refrigerant flow rate is that of the ejector diffuser outlet.

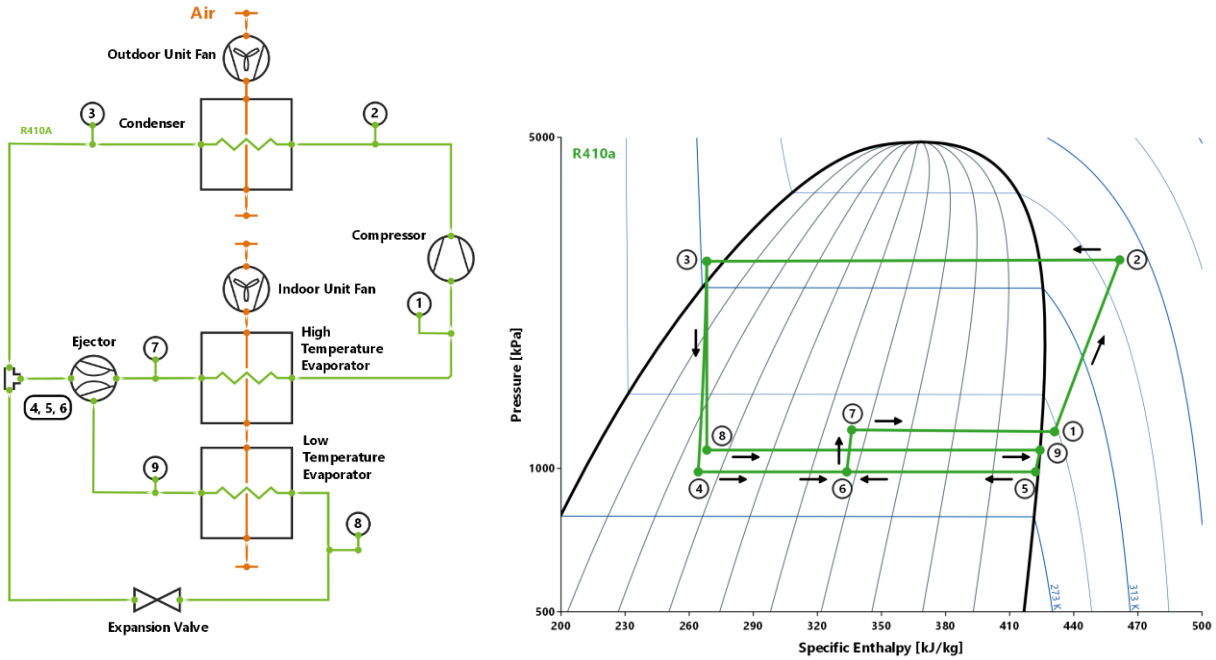

Figure 15: Condenser outlet split (COS) system– left: schematic, right: P-h diagram.

Another system which divides the refrigerant flow after the condenser is the condenser outlet split 2 system (COS2), described by Lee et al. (2000). In contrast to the COS cycle, where the ejector flows were two-phase, the COS2 cycle is a superheated vapor ejector cycle. The system schematic and its P-h diagram can be seen in Figure 16. A pair of expansion valves are employed which are fed refrigerant flow from the condenser. The ejector is placed downstream of a pair of evaporators. No liquid-vapor separator is used. The portion of the P-h diagram indicated with a black rectangle in the right side of Figure 16 is shown in more detail in Figure 17. Both evaporator outlet flows, points 5 and 10, as well as the ejector flows, are superheated vapor.

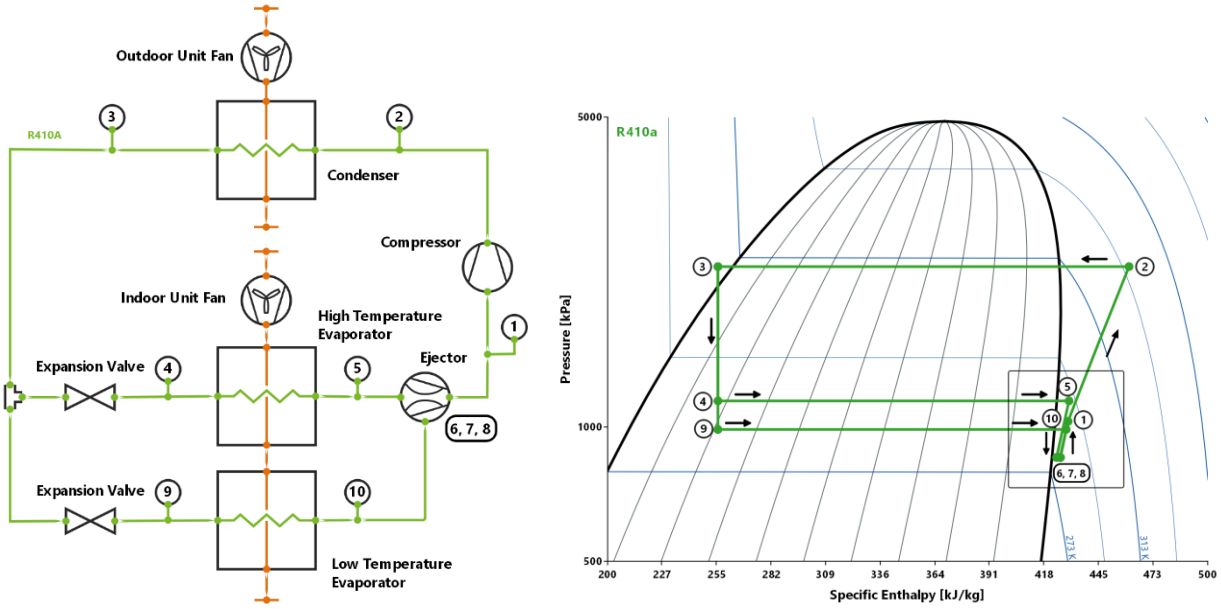

Figure 16: Condenser outlet split 2 (COS2) system – left: schematic, right: P-h diagram.

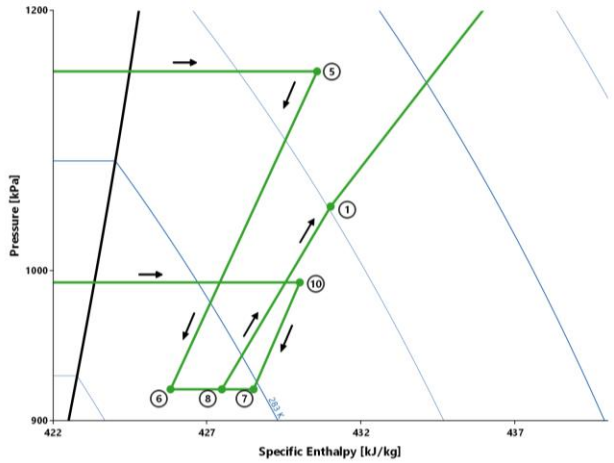

Figure 17: Condenser outlet split 2 (COS2) P-h diagram detail.

The two-phase diffuser outlet split (DOS) system was studied by Lawrence and Elbel (2013) and is shown in Figure 18. The DOS system uses the ejector as an expansion device. The refrigerant flow split occurs after the ejector at the diffuser outlet point 7, where the flow is routed to the high temperature evaporator then through a metering valve which reduces the pressure to the low temperature evaporator inlet at point 8. The two evaporators see parallel refrigerant flow. The metering valve and low temperature evaporator form a refrigerant flow recirculation loop. No liquid-vapor separator is employed.

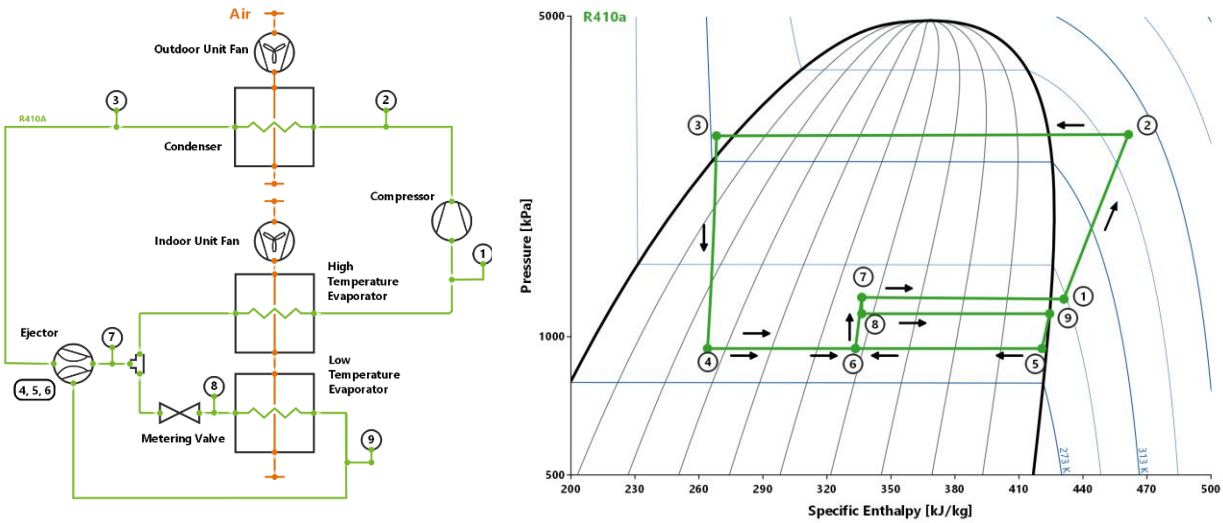

Figure 18: Diffuser outlet split (DOS) system – left: schematic, right: P-h diagram.

Tomasek & Radermacher (1995) studied the separator outlet split (SOS) ejector system in a refrigeration application. See Figure 19 for the schematic and P-h diagram. The system uses two expansion valves and the two evaporators are in series in the refrigerant flow. A liquid-vapor separator divides the refrigerant flow (points 6 and 10) and feeds the ejector and the low temperature evaporator. The ejector diffuser outlet enters the compressor. The black rectangle in the right side of Figure 19 is shown in more detail in Figure 20. The SOS system refrigerant flows driving the ejector are saturated vapor.

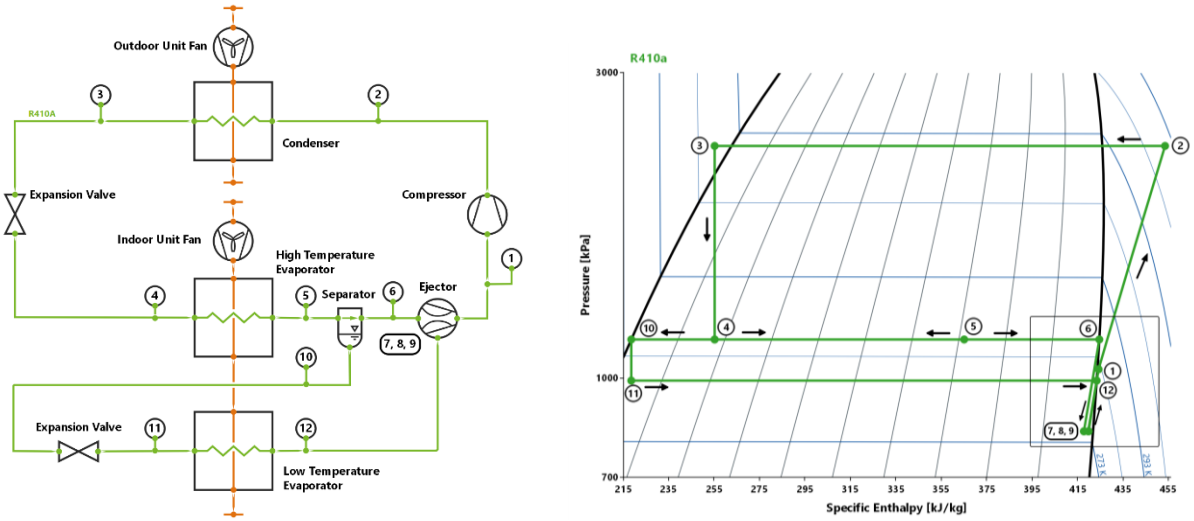

Figure 19: Separator outlet split (SOS) system – left: schematic, right: P-h diagram.

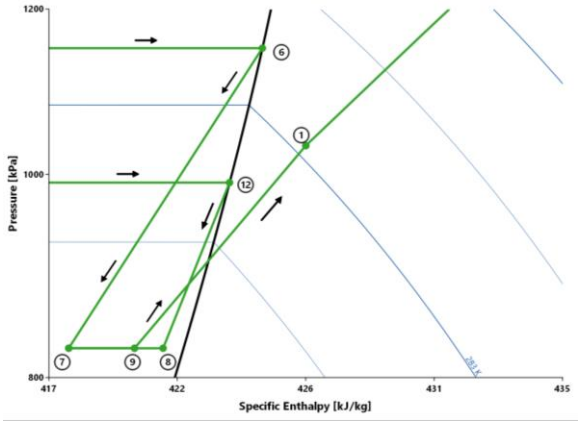

Figure 20: Separator outlet split (SOS) P-h diagram detail.

The separator outlet split 2 (SOS2) system, shown in Figure 21, was analyzed by Wang & Lyu (2014). Two expansion valves are utilized, and the two evaporators are in series in refrigerant flow. The branch in the refrigerant flow occurs at the liquid-vapor separator which feeds vapor to the compressor at point 1, and liquid to the second expansion valve at point 10. The primary flow to the ejector is two-phase refrigerant and the secondary flow is either saturated or superheated vapor.

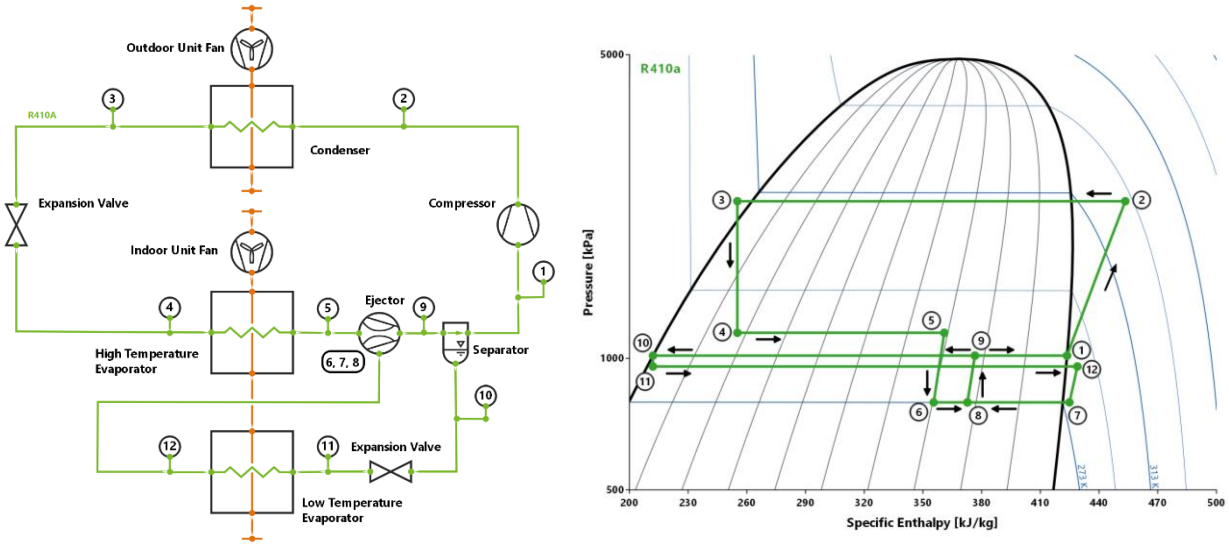

Figure 21: Separator outlet split (SOS2) system – left: schematic, right: P-h diagram.

The separator outlet split (SOS3) system is shown in Figure 22. The system is a hybrid of the standard two-phase ejector cycle and a dual evaporator vapor compression system. The ejector is used as an expansion device, however, in addition there are two expansion valves and a metering valve. The two evaporators are in parallel in

the refrigerant flow. The liquid-vapor separator feeds the compressor at point 1 and expansion valves at point 8. Both evaporators are in a refrigerant recirculation loop.

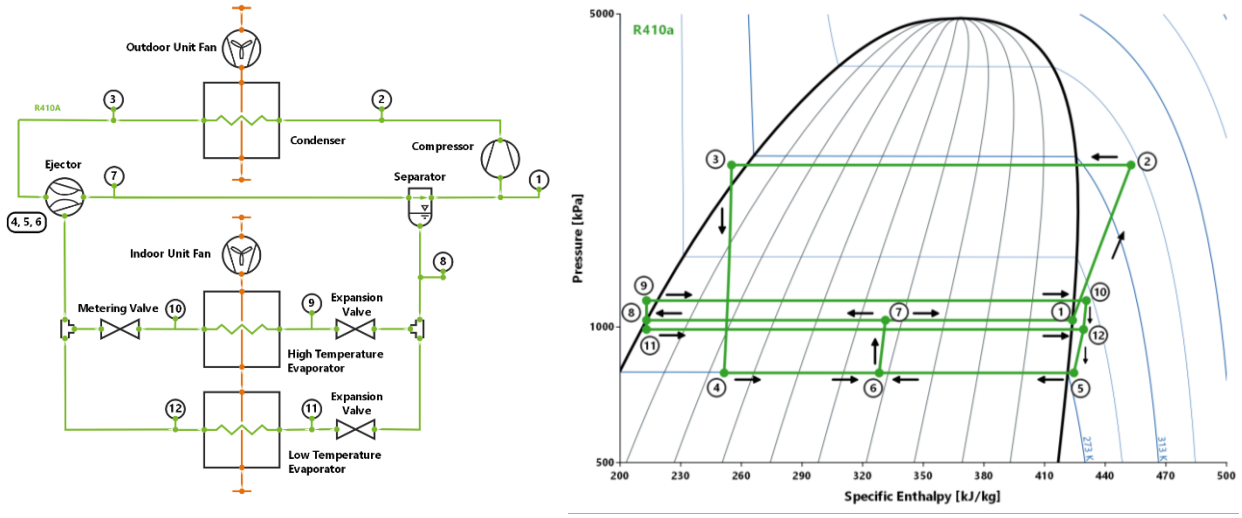

Figure 22: Separator outlet split (SOS3) system – left: schematic, right: P-h diagram.

A summary of details and components for each cycle introduced in this section of the report and considered with the simplified modeling approach is given in Table 12.

Table 12: Summary of ejector cycle configurations.

Cycle Type	System / Cycle	Ejector Fluid Phase	Evap.(s)	Evap. Refr. Arrangement / Recirc.	Expansion Valve(s)	Metering Valve	Liquid-Vapor Separator	Reference
Standard two-phase ejector cycle	Standard Ejector	Two-Phase	1	-	-	-	1	Lawrence and Elbel (2013)
Condenser outlet split	COS	Two-Phase	2	Parallel	1	-	-	Lawrence and Elbel (2013)
	COS2	Superheated Vapor	2	Parallel	2	-	-	Lee et al. (2000)
Diffuser outlet split	DOS	Two-Phase	2	Parallel / Recirc.	-	1	-	Lawrence and Elbel (2013)
Separator outlet split	SOS	Saturated vapor	2	Series	2	-	1	Tomasek & Radermacher (1995)
	SOS2	Two-Phase	2	Series / Recirc.	2	-	1	Wang & Lyu (2014)
	SOS3	Two-Phase	2	Parallel / Recirc.	2	1	1	

3.4.4. Results & Ejector Cycle Concept Screening

The simplified modeling approach described in Section 3.1.4, and the exergy analysis described in Section 3.1.5, were applied to the seven ejector enhanced vapor compression systems described in the previous section of the report. The purpose of the analysis was to identify viable candidate cycles for further study using the detailed modeling approach.

The COP and compressor compression ratio (CR) for the ejector system candidates and the dual evaporator systems are shown in Figure 23, normalized by the values of the baseline. Note the COP in the case of the simplified models included only the compressor power. The systems are ordered left to right from highest to lowest normalized COP. COP improvement was negatively correlated with CR, since decreased CR leads to improved COP due to the pressure lift generated by the ejector. In agreement with the analysis from Lawrence and Elbel (2013), the COP of the standard two-phase ejector, COS, and DOS cycles were all found to be equivalent with COPs of 6.73 (1.07 normalized), compared to the baseline COP of 6.27. The standard two-phase ejector, COS, and DOS cycles performed 7.3% better than baseline, while all other cycles were found to perform poorer.

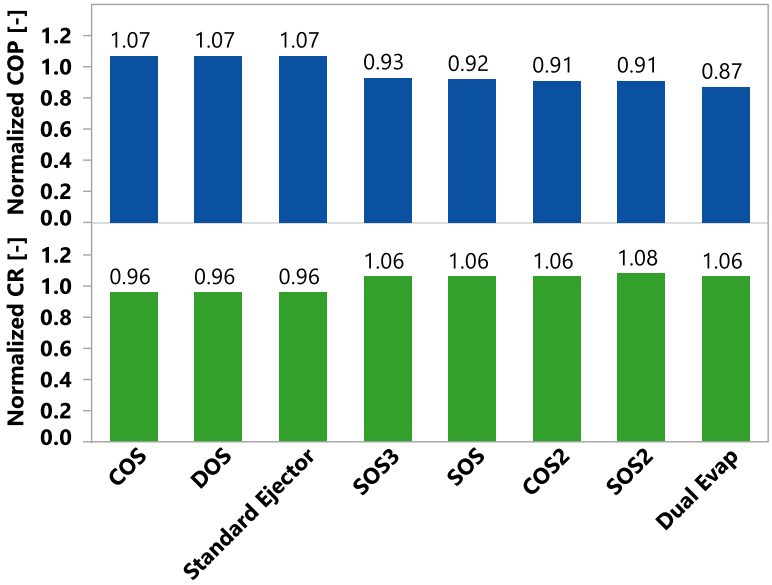

Figure 23: COP & CR for all ejector systems.

All of the dual evaporator ejector enhanced cycles performed better than the traditional dual evaporator vapor compression cycle discussed in Section 3.3. The best performing ejector enhanced cycles had COPs 20.7% higher than the dual evaporator cycle. The model runs and analysis for the baseline and standard two-

phase ejector cycle were repeated with R290 (propane) and R600a (isobutane) refrigerants which have higher expansion losses than R410A. Analysis showed the ejector provided an additional 2 to 4% COP improvement above R410A with these natural refrigerants.

Results of the exergy analysis are shown in Figure 24. Here the exergy destruction of the components found within the AHU are shown stacked. The total exergy destruction, represented by the height of the bars, suggests a performance metric for the AHU. The bars are ordered from highest to lowest exergy destruction. As expected, the dual evaporator has the highest exergy destruction with a significant portion coming from the expansion valves. In the case of the ejector cycles, the ejector accounts for some exergy destruction, however, the expansion losses can be seen to be lower in every case. Recalling the trends in the previous figure, and comparing to Figure 24, it can be seen that the AHU exergy destruction is positively correlated with the compressor CR and negatively correlated with the COP. The best performing cycles from an exergy destruction standpoint were COS and DOS. The combined exergy destruction in the evaporators for the COS and DOS cycles was 31% less than the evaporator exergy destruction in the baseline, standard two-phase ejector, and all other ejector cycles. The high temperature evaporator exergy destruction in the COS and DOS cycles was 61% less than all other ejector cycles.

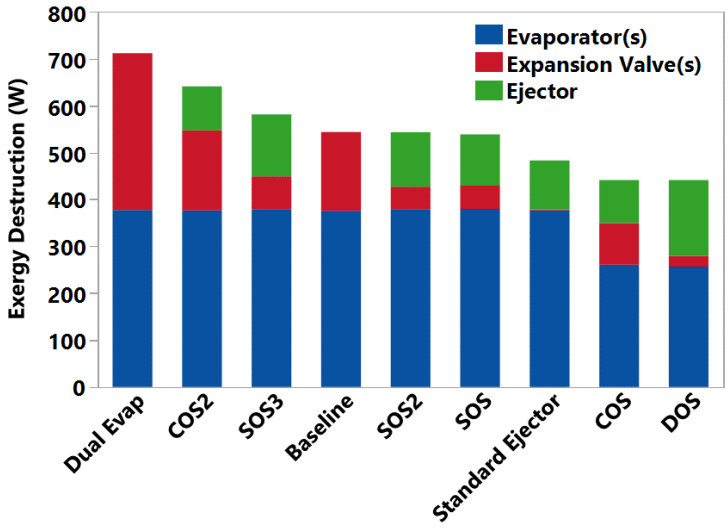

Figure 24: Comparison of AHU exergy destruction.

3.4.5. Evaluation of Selected Ejector Enhanced Concepts

The three cycles whose COP was higher than baseline, namely the standard two-phase ejector, COS, and DOS cycles were selected for further analysis with the detailed modeling approach discussed in Section 3.1.6 and the ejector physics represented by the modeling approach discussed in Section 3.4.2.

For the baseline cycle and the standard ejector cycle, both having a single evaporator, the UA correlations derived for the existing A-coil were used. For the COS and DOS cycles with dual evaporators the UA correlations derived for a single A-coil slab were employed for each evaporator. The single slab correlations were found from regressions of parametric runs in CoilDesigner®. The evaporator inlet refrigerant vapor quality was included as a parameter as the ejector enhanced cycles have a range of evaporator inlet qualities. For the condenser, the UA value correlations were found from regression of parametric runs in CoilDesigner® over a range of refrigerant mass flows and outdoor air inlet temperatures.

As shown previously in the schematics, the air flow through the evaporators was taken to be in series with the high temperature evaporator placed in the air flow path upstream of the low temperature evaporator.

The 10-coefficient compressor model was used in the baseline cases and the resulting compressor efficiencies were applied in the alternative cycle cases.

Based on the AHRI Standard 210/240 (AHRI, 2017), simulations were conducted at three different condenser air inlet temperatures: 28°C, 35°C, and 43°C; and 44% relative humidity to represent different outdoor ambient conditions. The indoor ambient condition, which is the evaporator air inlet condition, was held constant at 27°C and 50% RH, respectively.

The coefficient of performance used in the detailed analysis included the effect of capacity loss and the parasitic power of the indoor and outdoor blower/fan motors:

$$COP_{total} = \frac{\dot{Q}_{evap} - \dot{Q}_{loss}}{\dot{W}_{total}} \tag{23}$$

where $\dot{W}_{total} = \dot{W}_{comp} + \dot{W}_{fan}$. The capacity loss $\dot{Q}_{loss}$ was taken to be equal to the indoor fan power and $\dot{W}_{fan}$ was taken as the sum of the indoor and outdoor blower/fan powers.

Compressor displacement for each alternative cycle was modified by a scaling factor, F_{size}, where a value of one represents the baseline, in order to match each cycle's cooling capacity to the respective baseline case. A sum of squares error minimization approach was used to find the appropriate value of the compressor scaling parameter and iterating during model runs (Table 13).

Table 13: Compressor scaling factor values.

Compressor Scaling Factor [-]	Ambient Temperature [°C]		
	28	35	43.33
Standard Ejector	0.97	0.93	0.93
COS	0.96	0.92	0.88
DOS	0.93	0.91	0.89

The effect of the ejector on the compressor suction temperatures is shown in Table 14. The ejector increased the suction temperature above baseline for all ejector cycles and all ambient temperature cases. The largest temperature increase was observed in the DOS cycle, followed by the COS cycle, lastly the standard two-phase ejector cycle. These temperature increases correspond with reduced approach temperatures in the high temperature evaporator.

Table 14: Suction temperatures.

Suction Temperature [°C]	Ambient Temperature [°C]		
	28	35	43.33
Baseline	10.2	10.8	11.7
Standard Ejector	11.5	13.3	15.4
COS	16.5	18.5	20.6
DOS	17.6	18.8	20.8

Table 15 lists the refrigerant mass flows obtained from the models for all cycles compared to baseline at each outdoor ambient condition. For the COS and DOS cycles the designators high and low indicate the high temperature and low temperature evaporators, respectively. The standard ejector cycle refrigerant mass flow rates generally matched the baseline, while the high temperature evaporators in the COS and DOS cycles have refrigerant mass flow rates comparable to the

baseline. The refrigerant mass flow rates through the low temperature evaporators are lower than those through the high temperature evaporator in both the COS and DOS cycles. The COS cycle low temperature evaporator refrigerant mass flow rates are 55 to 59% lower than the those through the high temperature evaporator. The refrigerant mass flow rates for the low temperature evaporator in the DOS cycle are 18 to 23% lower than those through the high temperature evaporator.

Table 15: Evaporator mass flow rates.

Evaporator Refrigerant Mass Flow [g/s]		Ambient Temperature [°C]		
		28	35	43.33
Base		64.0	64.8	65.5
Standard Ejector		63.9	64.7	66.4
COS	High	63.9	64.7	65.1
	Low	28.8	28.1	26.6
DOS	High	63.9	64.7	66.4
	Low	52.7	50.0	51.3

The SHR from the baseline model cases ranged from 0.76 to 0.81. The standard ejector cycle SHR across the ambient conditions deviated from baseline by -0.5% to +1.6%. For the COS and DOS cycles a mass flow average SHR was calculated. The COS cycle SHR deviated -4.2% to +1.8%, and the DOS cycle SHR deviated -0.4% to -1.7% from baseline. The SHR for each evaporator in the COS and DOS cycles are shown in Table 16. The higher the outdoor ambient temperature, the more the high temperature evaporator acts as a sensible HX. The DOS cycle high temperature evaporator tends to have higher SHR compared to the COS cycle. The low temperature evaporators operate with lower SHR, however, they are not solely latent HXs. The SHR for the low temperature evaporators ranged from 0.561 to 0.681, depending on the cycle and the ambient temperature. This suggests there is room for design improvement in the ejector enhanced systems to advance further towards a true SSLC system.

Table 16: Comparison of COS & DOS evaporator SHR.

SHR [-]	Cycle	Ambient Temperature [°C]		
		28	35	43.33
High Temp. Evaporator	COS	0.764	0.902	0.997
	DOS	0.846	0.920	1.000
Low Temp. Evaporator	COS	0.681	0.594	0.561
	DOS	0.642	0.604	0.582

The percent change in compressor power, CR, and COP total for the standard two-phase ejector, COS, and DOS cycles at each outdoor ambient temperature are shown in Figure 25.

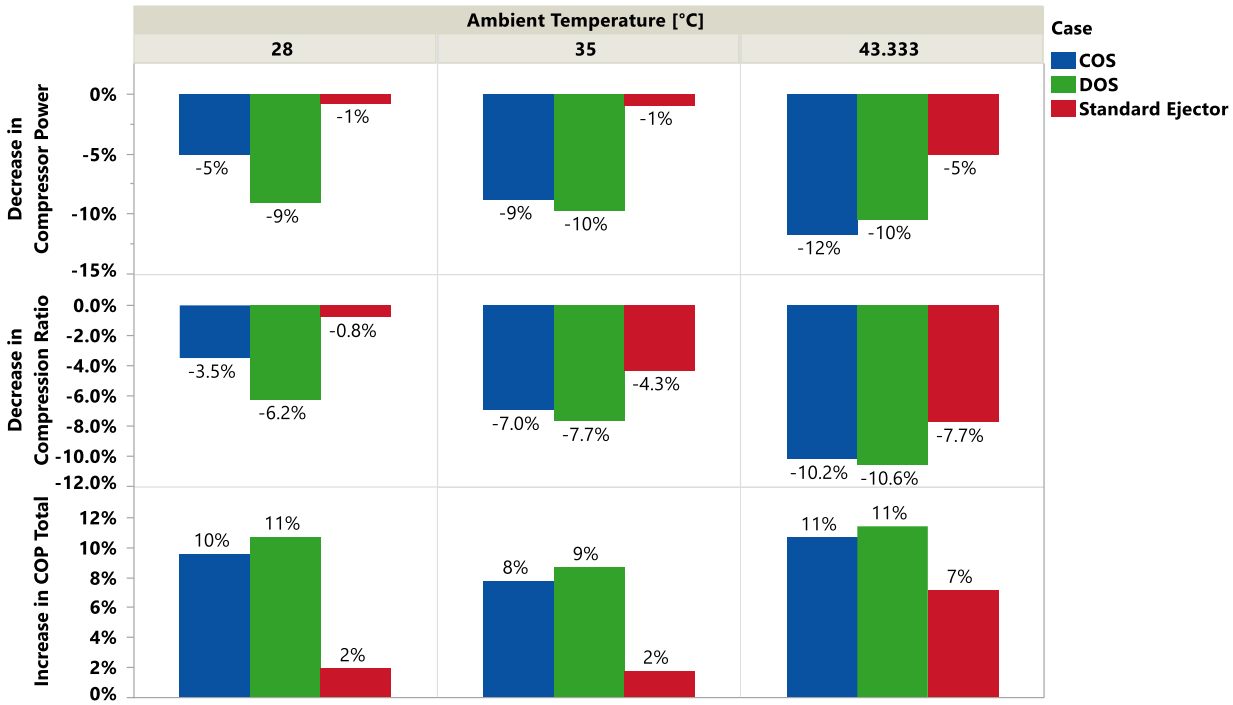

Figure 25: Comparison of compressor power, CR, and COP total.

The percent improvement in COP total for the COS & DOS cycles ranged from 8 to 11% across the ambient temperatures. The standard two-phase ejector cycle performed comparatively poorer, with COP total improvements of 2 to 7% across the ambient temperatures. The improvement in COP total in these cycles was driven by the reduction in compressor power due to a reduction in compression ratio enabled by the ejector.

The percent increases in SEER above the baseline model result of 15.34 are shown in Figure 26. The DOS cycle was found to perform most favorably with an 8% increase in SEER, followed by COS with a 4% increase. The difference in SEER between the COS and DOS cycle was due to 3.4% lower total power consumption for the DOS cycle compared to the COS cycle at the 28°C rating point. Lastly, the standard ejector cycle had only a 1% increase in SEER over baseline.

A comparison of the exergy destruction in the indoor unit (AHU) and the outdoor unit for the baseline, COS, and DOS systems is shown in Figure 27 at the three outdoor

ambient temperature conditions. The indoor unit (AHU) components are shown in the upper row, while the outdoor unit components are shown in the lower row.

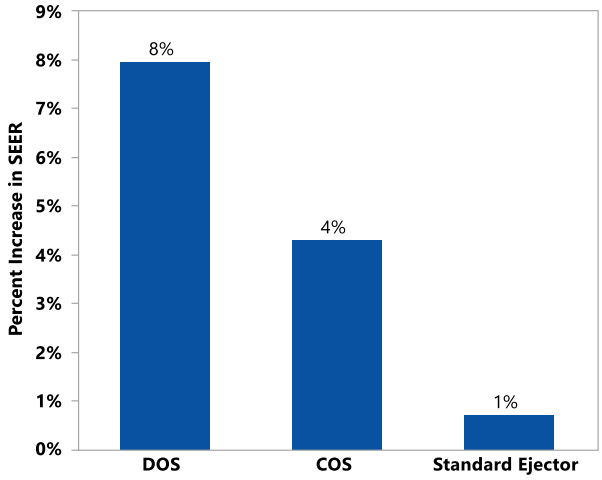

Figure 26: Percent increase in SEER.

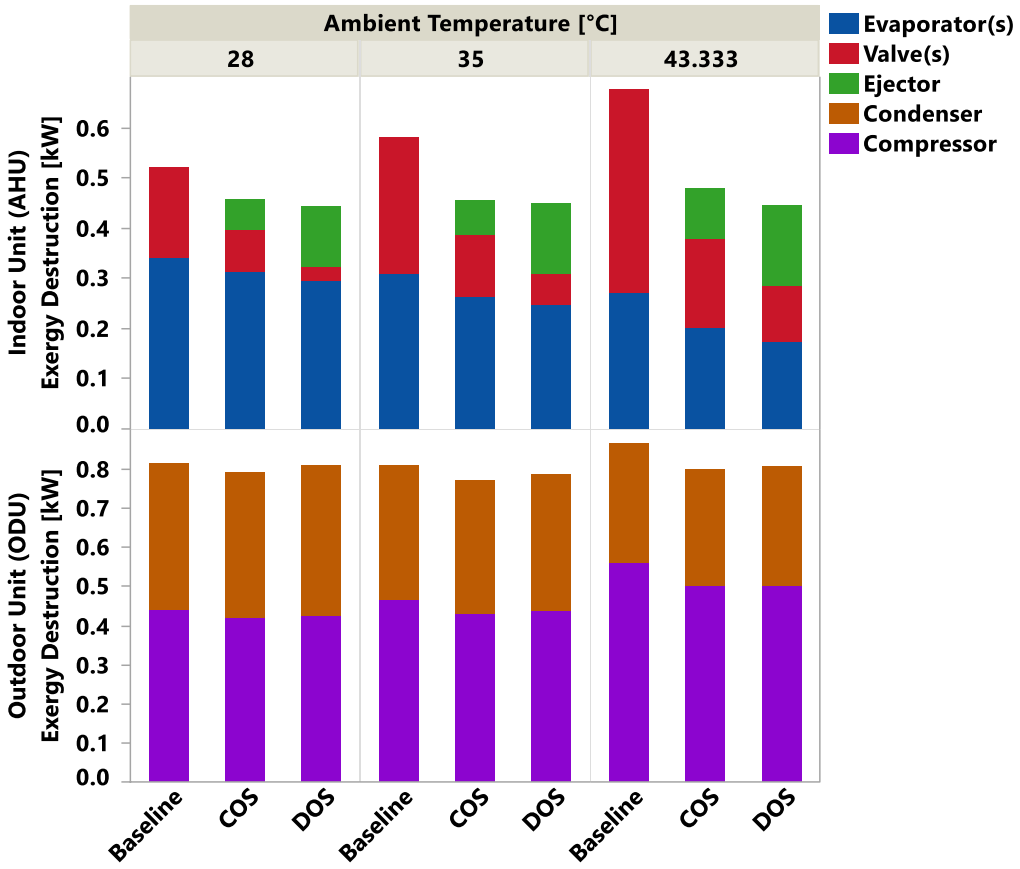

Figure 27: Exergy destruction in AHU & outdoor unit.

Starting with the indoor unit, the expansion losses increased with increasing outdoor ambient temperature. The ejector enhanced cycles show lower expansion losses relative to the baseline at all ambient temperatures. Evaporator losses decreased with increasing outdoor ambient temperature, due to rising evaporating temperatures.

Moving to the outdoor unit, the losses at the condenser increased with increasing outdoor temperature. Within a given ambient temperature the condenser losses remained similar regardless of the type of system. The positive effect of the ejector on compressor losses can be seen in the outdoor unit portion of the graph.

The percent reduction in exergy destruction in the AHU and the ODU against the baseline is shown in a grid of graphs in Figure 28 for the COS and DOS cycles at each outdoor ambient temperature. It is clear these ejector enhanced cycles had reduced losses in both the AHU and the ODU, and that the reduction in losses increased with increasing outdoor temperature. The loss reduction was greater in the AHU compared to the ODU. The reduction in losses in the ODU was primarily driven by compressor load reduction, which was a consequence of higher suction temperatures afforded by the ejector. Improvement in AHU losses ranged from 10 to 29% for the COS cycle, and from 12 to 36% for the DOS cycle.

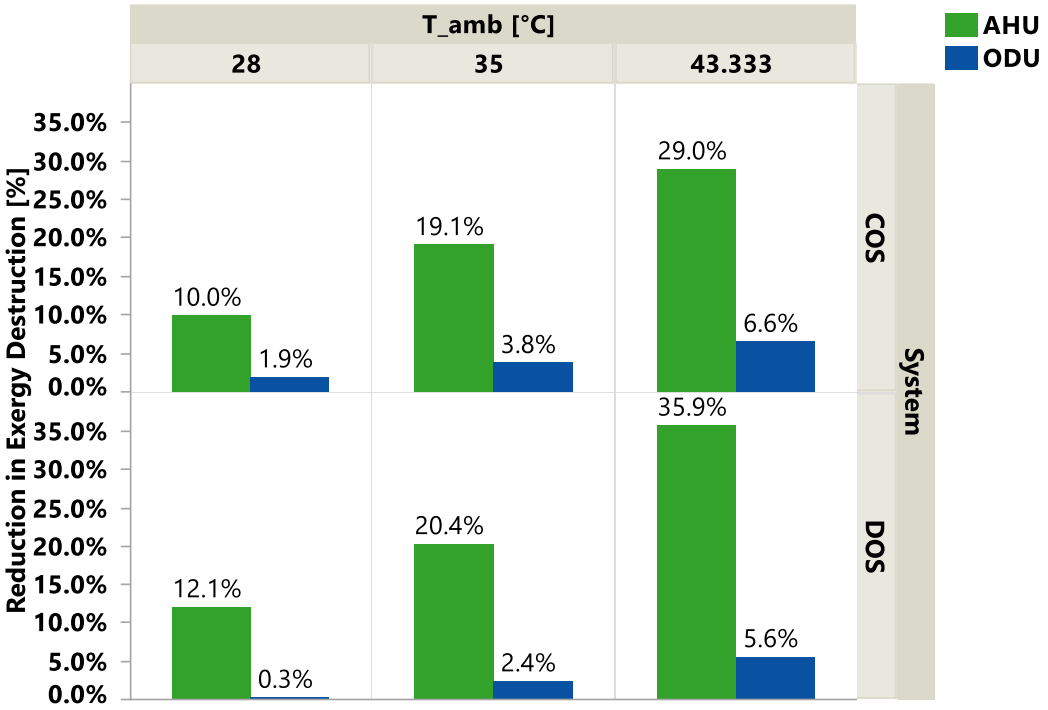

Figure 28: Percent reduction in exergy destruction.

3.4.6. Coil Concepts, Analysis, and Optimization

Four potential HX designs for ejector enhanced dual evaporator AHUs are:

1) Existing A-coil with each slab divided into two evaporator refrigerant circuits, series air flow.

2) Existing A-coil with each slab acting as an independent evaporator, parallel air flow.

3) Single angled slab divided into two evaporator refrigerant circuits, series air flow.

4) Single perpendicular slab divided into two evaporator refrigerant circuits, series air flow.

The baseline A-coil refrigerant flow was divided for each coil slab. Since the total refrigerant mass flow through a HX slab in the ejector enhanced systems can be higher than baseline, any candidate design must implement a refrigerant circuit configuration intended to manage refrigerant side pressure loss.

Design 1 has the advantage of minimal changes required compared to the baseline A-coil, and no expected impact on air side pressure loss. Design 2 has a detrimental reduction in air flow rate to the evaporators since the airflow is in parallel compared to series in the other cases.

Designs 1, 3, and 4 have series air flow configurations which has the advantage of cooling the indoor air with the high temperature (sensible) evaporator before it is passed through the low temperature evaporator.

Designs 3 and 4 have the challenge of reduced face area which could impact heat transfer and increase air side pressure loss if steps are not taken during design to mitigate these issues. Design 4, however, has the ability for significantly increased coil depth which allows additional tube banks and wider fin pitch to manage the heat transfer and air side pressure losses. Designs 3 and 4 create opportunity to significantly reduce HX material, which in the case of the baseline AHU A-coil, is aluminum. A significant reduction in refrigerant charge would also result. Reduced material and refrigerant charge would reduce cost and offset part of the added cost of the ejector or other added components.

Design 3, the angled slab-coil HX, was developed with CoilDesigner® for use in the COS and DOS ejector cycles which require dual evaporators. Compared to the existing AHU A-coil the angled-slab design had the same number of tube banks (4), and the fin type/details and tube enhancements were also kept the same as baseline. In this design the first pair of banks form the refrigerant circuit for the high temperature evaporator, and the second pair of banks form the refrigerant circuit for the low temperature evaporator. The available space in the AHU allowed the number of tubes per bank to be increased from 22 to 25. As mentioned, circuiting must be done in such a way as to manage the refrigerant side pressure drop.

Designs for the A-coil and an angled-slab coil, shown in Figure 29, were analyzed with CoilDesigner® and compared. Inlet air and refrigerant states and mass flows were set according to outputs from the detailed EES models. The refrigerant states were specified with saturation pressure and quality. For the baseline case the analysis was conducted for a single slab of the A-coil, and where appropriate results were doubled to represent the two A-coil HX slabs. In the COS and DOS cases analysis was first conducted for an upstream circuit for the high temperature evaporator. The output states of the air and refrigerant were then applied as the inlet states to the downstream low temperature evaporator. Results from each pair of analyses were combined for the high and low temperature evaporators in the COS and DOS cases. Results are given in Table 17.

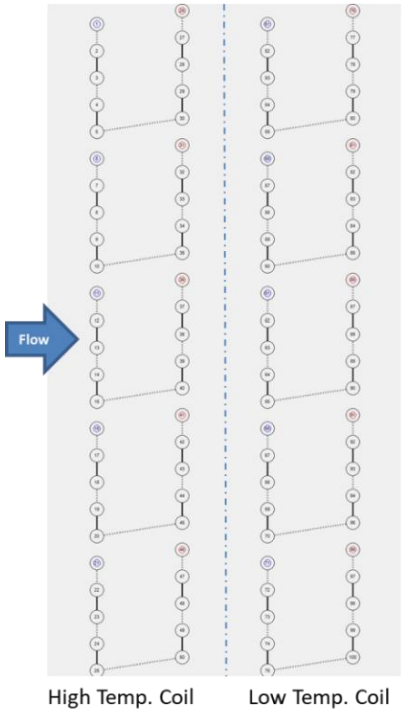

Figure 29: Angled-slab coil design tube layout.

Table 17: Angled-slab coil analysis results.

		A-Coil	Angled Slab	
			COS	DOS
Heat Loads	Total Heat Load [kW]	10.895	11.609	11.478
	Sensible Heat Load [kW]	8.382	9.205	8.594
	Latent Heat Load [kW]	2.514	2.404	2.885
	Sensible Heat Ratio [-]	0.769	0.793	0.749
Charge/Condensate	Total Refrigerant Charge [kg]	0.308	0.163	0.124
	Condensate [kg/s]	0.00102	0.00097	0.00117
Flow Rate	Slab Refrigerant Flow Rates [g/s]	31.5/31.5	64.7/28.5	64.7/50.8
Pressure Drops	HX Air Side Pressure Drop [Pa]	24.6	56.6	56.7
	Refrigerant Side Pressure Drop [Pa]	9876	22135	31778
Heat Transfer	Primary Heat Transfer Area [m^2]	2.12	1.20	1.20
	Secondary Heat Transfer Area [m^2]	33.99	19.31	19.31
	Total Air Side Heat Transfer Area [m^2]	36.10	20.51	20.51
	Ref. Side Heat Transfer Area [m^2]	1.88	1.07	1.07
	Ref. Side Area Enhancement [-]	1.91	3.81	3.81
	Coil Face Area [m^2]	0.47548	0.53976	0.53976
HX Material	Fin Material Volume [m^3]	0.00203	0.00114	0.00114
	Tube Material Volume [m^3]	0.00157	0.0009	0.0009
	Fin Material Mass [kg]	5.48	3.06	3.06
	Tube Material Mass [kg]	4.24	7	2.41
HX Dimensions	Coil Length [m]	0.425	0.425	0.425
	Coil Depth [m]	0.0762	0.0762	0.0762
	Coil Height [m]	1.118	0.635	0.635

The angled-slab coil had higher total capacity compared to the A-coil. The material mass was reduced 44% compared to the A-coil, and refrigerant charge was reduced 47 to 60%. The issues noted earlier with increased air side and refrigerant pressure drops were evident with an increase in air side pressure loss of 56%, and refrigerant side pressure loss increase on the order of 200-300%.

A genetic algorithm used in conjunction with CoilDesigner® was applied to generate and screen 40,000 additional alternative candidate HX designs with 7 mm and 9.5 mm tubes. Results showed that an optimized HX design with could limit air side and refrigerant side pressure loss increases to 4%, and 26%, respectively.

The single angled-slab HX, Design 3, was selected for analysis with CFD. The computational domain can be seen in Figure 30. The domain is like that described in Section 3.1.3; however, the geometry was modified. The A-coil was replaced with the longer, single angled-slab, and the drain pain area was modified accordingly to accommodate the single slab. A porous zone was added to represent the flow resistance of the coil, with the same porous media parameters used for both the A-coil and single slab investigations as fin details and coil depths were the same for both coils. A moving reference frame modeled blower rotation which was set to rotate at 800 rpm. Fluid properties were set to constant density and viscosity, and turbulence was evaluated using a k-ε realizable model with enhanced wall treatment. The modified CFD geometry was meshed in ANSYS Fluent with a poly-hexcore mesh having 1.06M cells.

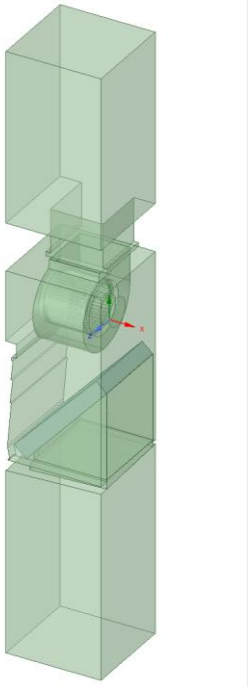

Figure 30: Computational domain of angled slab coil.

The velocity vectors in the AHU near the angled slab coil are shown in Figure 31. In comparison to Figure 7, Figure 31 shows lower velocities around the coil inlet due to the increased flow area of the reconfigured drain pan and relatively lower velocities on the walls of the air handler, reducing friction. The angled slab geometry lacks the airflow deflector present in the A-coil design, smoothing the airflow path from the coil outlet to the blower. The velocity vectors within the coil and at the coil outlet were relatively consistent in magnitude, which was confirmed by the velocity distributions at the coil surface derived from CFD results. The velocity distributions at the outlets for both the angled slab and A-coil HXs and are shown in Figure 32.

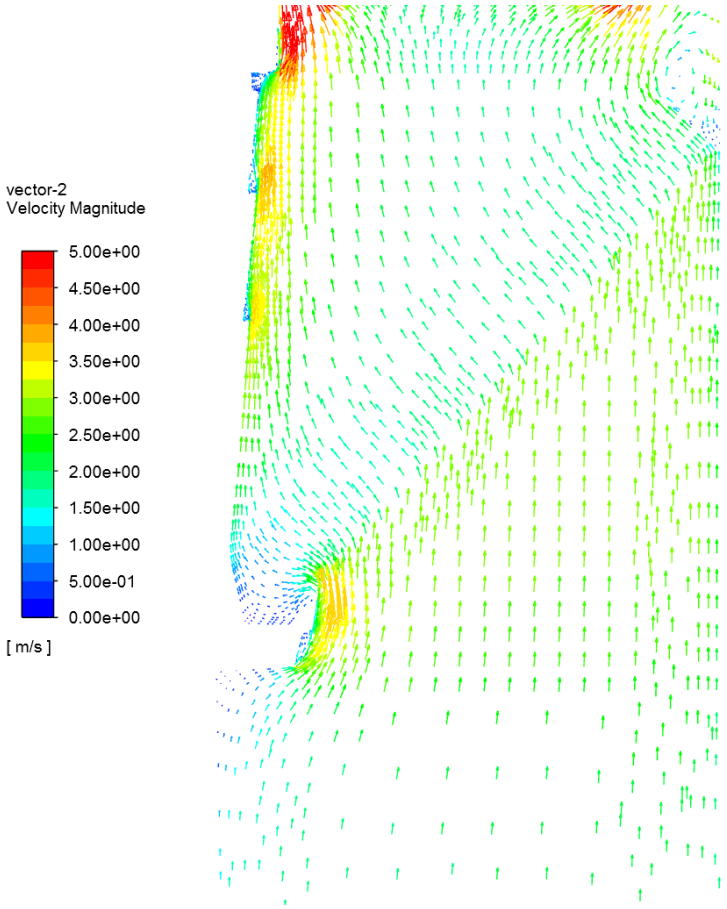

Figure 31: Velocity Vectors in cross-section of the AHU near the angled slab coil.

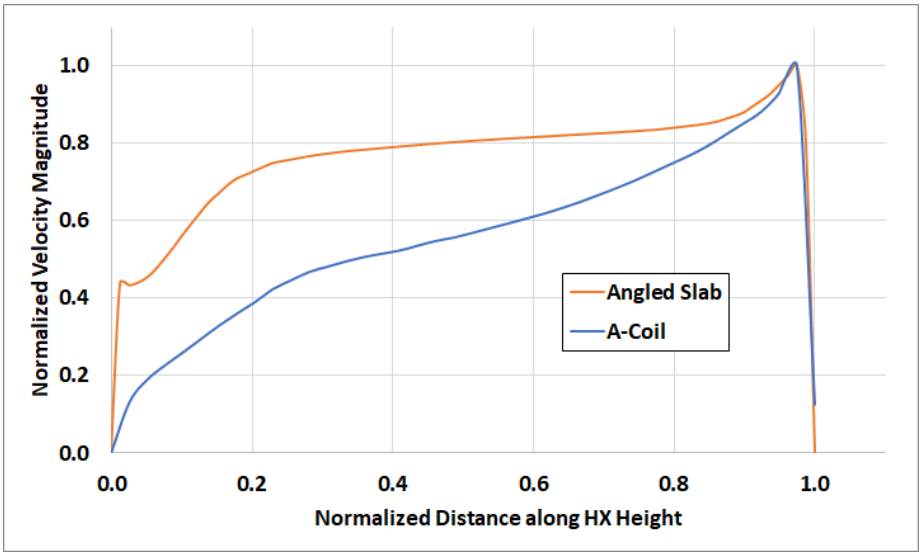

Figure 32: Velocity profiles at outlet of angled slab & A-coil.

The normalized velocity magnitude shows a greatly improved airflow distribution across the coil outlet of the angled slab versus the A-coil. Overall, velocities tended to be more uniform in magnitude along the height of the HX. The angled-slab configuration allowed for improved air flow distribution across the coil and increased net air flow rate through the air handler at 800 rpm blower speed. It is expected that this improved velocity distribution would result in modest performance gains and energy savings.

3.5. SSLC Concept with Desiccant Wheel

3.5.1. Introduction

Moisture removal from supply air requires a significant amount of energy, especially in hot and humid climates. Conventional AC systems rely on the evaporator to lower the air temperature below the dew point to achieve dehumidification. Separate sensible and latent cooling (SSLC) is one approach to improve the efficiency of AC systems and provide more accurate humidity control. By decoupling the thermal load into sensible latent and components, the sensible evaporator can operate at higher evaporating temperature which reduces compressor power consumption due to reduced compressor pressure ratio. Latent heat can be removed with a solid desiccant wheel (DW). The desiccant in the wheel is heated by adsorbing water vapor from the process air and further reheated by regeneration air. The regeneration desorbs moisture while heating the process air to a comfortable temperature.

Previous research on DW-assisted SSLC showed the technology capable of providing significant energy savings. Ling et al. (2011) experimentally evaluated a SSLC AC system composed of a vapor compression system with a DW regenerated by waste heat from the condenser. They used R-410A as the refrigerant in their experimental evaluations and varied desiccant regeneration temperature between 45°C and 55°C. Their evaluations showed overall COP enhancement between 7% and 34% dependent on regeneration temperature. They also observed that the latent load of the DW increased with increasing regeneration temperature, however the system COP decreased due to increased discharge temperature and compressor power input.

In this work, an AC system is proposed consisting of a vapor compression system using R-410A and a DW with a desiccant material based on AQSOA[1] Ferroalumino-phosphate Zeolite (FAM-Z01[2]) with 7.3 Å pore size (Mitsubishi Plastics, 2010). This material has a unique isotherm shape and has the characteristic of adsorbing moisture with a small change in relative vapor pressure as shown in Figure 33. This desiccant can also be regenerated using a low temperature heat source, as shown in Figure 34. The FAM-Z01 was selected to strike a balance between regeneration temperature and the amount of water vapor adsorbed. FAM-Z01 adsorbs less water vapor per unit mass of adsorbent than FAM-Z02, and can be regenerated using a lower temperature heat source. Even though FAM-Z01 adsorbs a similar amount of adsorbate as FAM-Z05, it starts the adsorption process at lower relative humidity, which is attractive for hot and humid weather conditions. The FAM-Z01 can be regenerated with a temperature source as low as 45°C, lower than that needed for other commonly used desiccant materials such as Silica-Gel (Al-Alili, 2015).

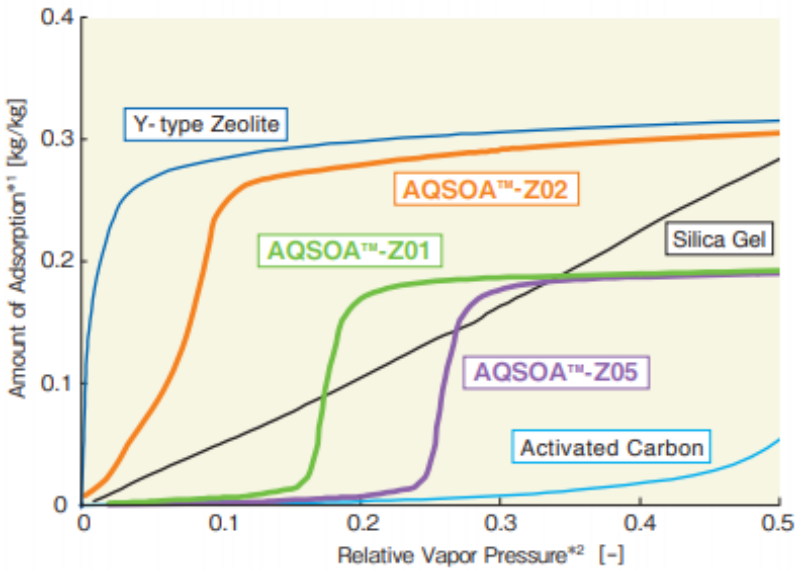

Figure 33: Isotherms of various desiccant materials (Mitsubishi Plastics, 2010)[3].

[1] AQua SOrb Zeolitic Adsorbent

[2] Functional Adsorbent Material Zeolite 01

[3] Amount of adsorption = amount of water [kg] which 1 kg of dried adsorbent can adsorb
Relative vapor pressure = relative humidity when the ambient air temperature is equal to the adsorbent temperature

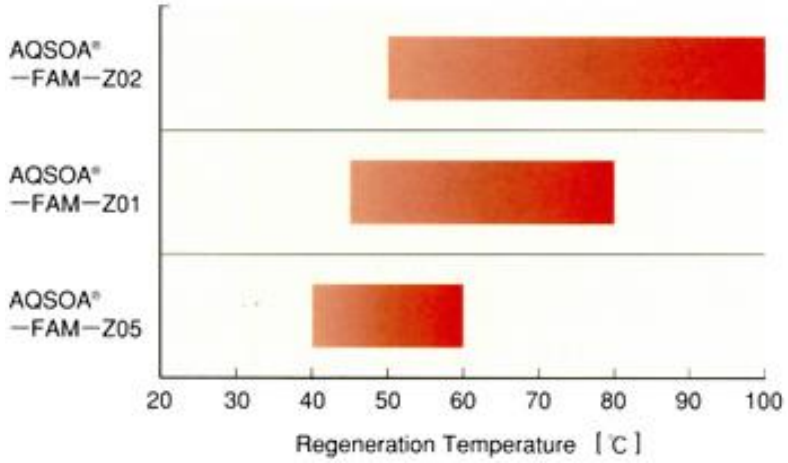

Figure 34: Recommended regeneration temperature (Mitsubishi Plastics, 2010).

3.5.2. Modelling Approach

Engineering Equation Solver (EES) was applied to investigate the performance of the DW-assisted SSLC system (Klein, 2020). Ten-coefficient models were used to calculate compressor refrigerant mass flow rates and power. The condenser and evaporator were modeled as counterflow HXs. The UA values were calculated by using refrigerant and air temperatures after simulating a range of air volumetric flow rates, refrigerant mass flow rates, as well as air and refrigerant inlet temperatures. Vapor quality was an additional variable for the calculation of the evaporator UA values. Linear curve fits for UA values were created by using results from parametric analyses conducted in CoilDesigner®.

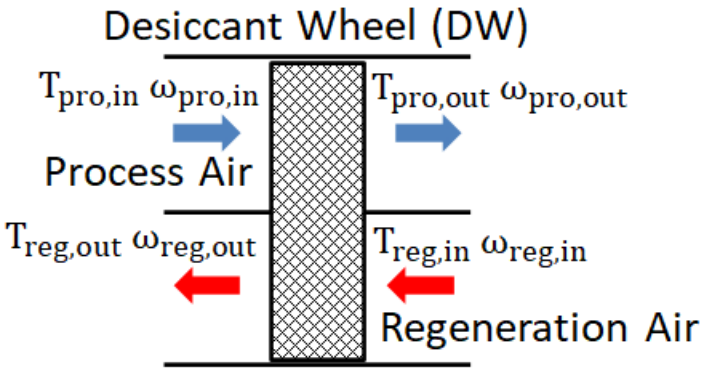

Figure 35: Desiccant wheel scheme (De Antonellis et al., 2015).

The performance of the DW shown in Figure 35 is based on the F_1 - F_2 iso-potential lines method. These iso-potential lines are functions of the wheel's inlet temperatures and humidity ratios, Equations 24 and 25. The outlet conditions of the supply air can be calculated using the effectiveness for each line, Equations 26 and 27. The values of η_{F_1} and η_{F_2} used in this simulation are 0.08 and 0.95, respectively, from Al-Alili et al. (2012).

$$F_{1,k} = -\frac{2865}{(T_k + 273.15)^{1.49}} + 4.344 \cdot (\omega_k)^{0.8624} \quad (24)$$

$$F_{2,k} = -\frac{(T_k + 273.15)^{1.49}}{6360} - 1.127 \cdot (\omega_k)^{0.07969} \quad (25)$$

$$\eta_{F_1} = \frac{F_{1,pro,out} - F_{1,pro,in}}{F_{1,reg,in} - F_{1,pro,in}} \quad (26)$$

$$\eta_{F_2} = \frac{F_{2,pro,out} - F_{2,pro,in}}{F_{2,reg,in} - F_{2,pro,in}} \quad (27)$$

For the DW-assisted SSLC system shown in Figure 36, the air flow rate through the evaporator was increased from 0.6 m^3/s to 0.922 m^3/s to avoid any air side moisture condensation in the evaporator and to remove additional sensible heat added to the process air by the DW. It was assumed that the latent capacity would be met by the DW, and the total system capacity would be the same as that of the baseline (conventional) system. The compressor displacement, mass flow rate, and power were scaled by a compressor size factor (F_{size}) which also indicated if the total system cooling load could be met by the existing compressor (F_{size} <= 1) or not (F_{size} > 1). The mass flow rate of process air through the DW was calculated using the latent heat load of the baseline AC, the humidity ratio inlet/outlet difference, and the enthalpy of the water evaporation. It was also assumed that process and regeneration air flow rates through the DW were equal. The desiccant in the DW was regenerated with heat from the condenser.

Based on the AHRI Standard 210/240 (AHRI, 2017), simulations were conducted at three different condenser air inlet temperatures (28°C, 35°C, 43°C) and 44% relative humidity, while evaporator air inlet temperature and relative humidity were kept constant at 27°C and 50%, respectively.

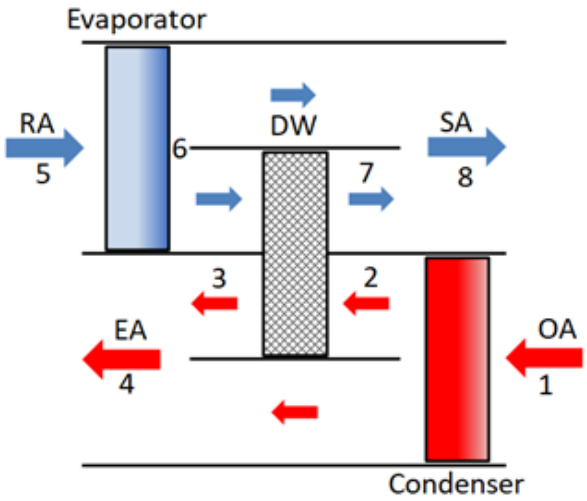

Figure 36: Airflow of DW-assisted SSLC system (Ling et al., 2011).

3.5.3. SSLC-DW Results and Discussion

To compare the SSLC-DW to the baseline system, Figure 37 illustrates changes in evaporating, condensing, and supply air temperatures at different ambient temperatures. The increase of evaporating and condensing temperature was lowest at the highest ambient temperature and highest at the lowest ambient temperature. Thus, it would be expected that the compressor pressure ratio and consequently the compressor power would be the lowest at the highest ambient temperature. The supply air temperature was 4 K to 4.4 K higher than that of the baseline system, attributed to increased evaporating temperature as well as additional sensible load imposed by the DW. The increase of the supply air temperature at different ambient temperatures differed marginally (below 0.4K).

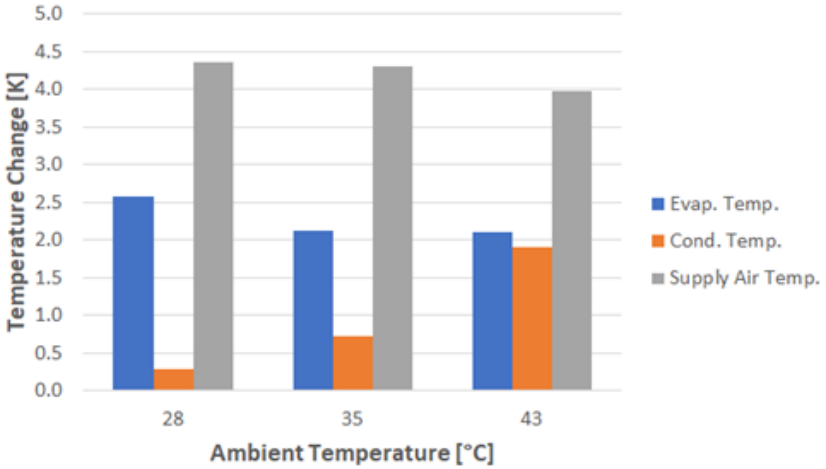

Figure 37: Evaporating, condensing, and supply air temperature change.

Figure 38 shows changes in COP, and compressor power and size compared to the baseline system at different ambient temperatures. It was clear that the compressor power ratio was lower at the 28°C and 35°C ambient temperatures due to increased evaporating temperature. However, the compressor power ratio was greater than one at the 43°C ambient temperature, which indicated that the existing compressor would not be able to meet the increased latent load added to the process air by the DW. The COP is lower than that of the baseline system at all ambient temperatures. The decrease in COP was caused by increased evaporator fan power consumption due to required higher air flow rate. In addition, the COP decreased at 43°C because of increased compressor power.

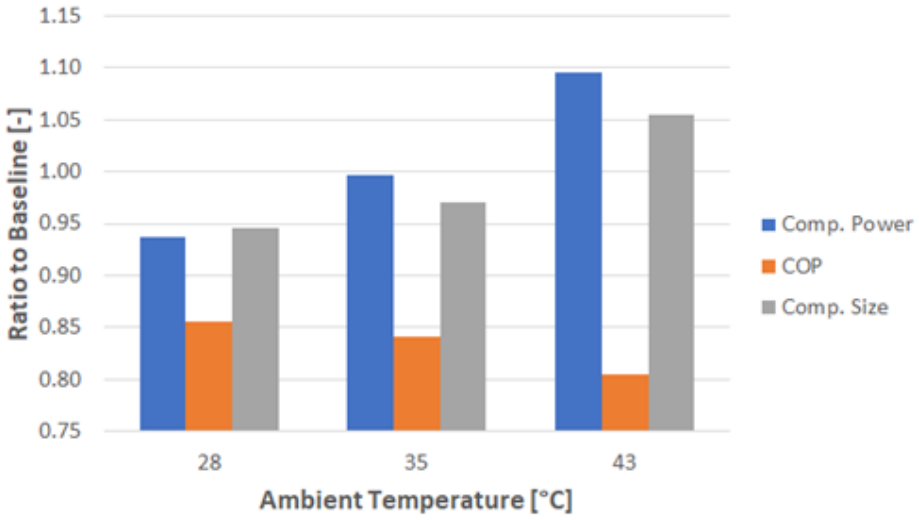

Figure 38: Compressor power, system COP, & compressor size.

Additional parametric analysis was conducted to investigate the effects of evaporating temperature on system performance. Figure 39 shows the compressor and total power consumption of the baseline and DW assisted SSLC systems. The compressor power consumption of the baseline system and the initial compressor power consumption of the SSLC system are nearly the same. The compressor power consumption was found to decrease with increasing evaporating temperature. However, the decrease of the compressor power consumption marginally affected total power consumption for the system because of the increased evaporator fan power consumption due to the required higher air flow rate. Figure 40 shows that the evaporating temperature of the SSLC system needs to be higher than 17 °C to have a comparable COP with the baseline system.

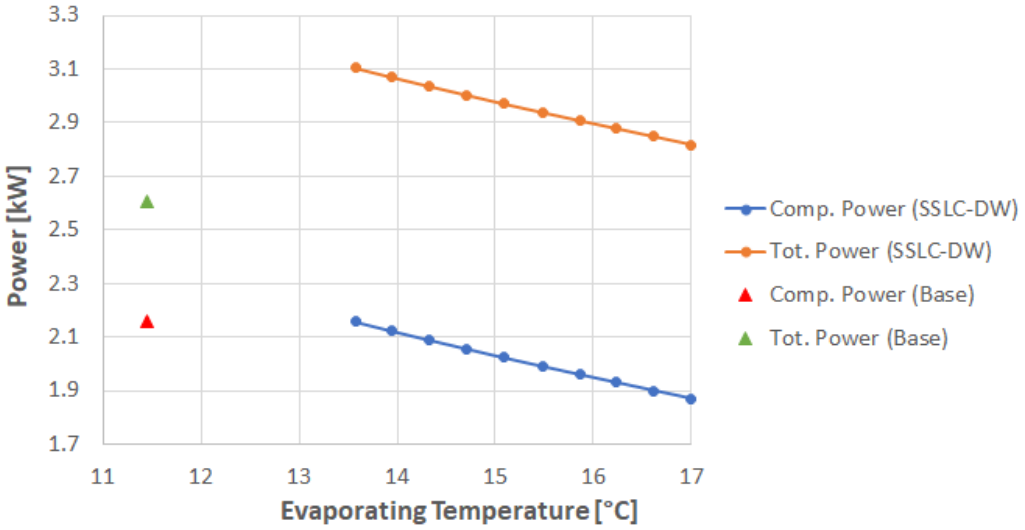

Figure 39: Effect of evaporating temp. on comp. & system power (Ambient temp. 35°C).

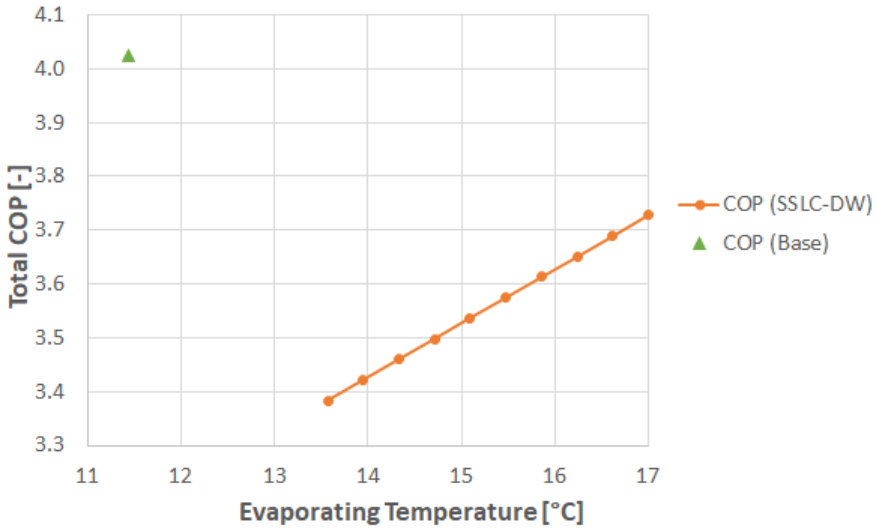

Figure 40: Effect of evaporating temp. on total COP (Ambient temp. 35°C).

To explore a more efficient DW assisted SSLC system, the effects of the regeneration and process inlet temperature on DW performance were examined. The goal of the analysis was to find more favorable conditions for DW operation. Figure 41 illustrates the ratio of the sensible to latent heat of the DW. This ratio decreased with increasing regeneration air temperature at low process air inlet temperatures up to approximately 27 °C. At higher process air temperatures, the ratio remained nearly constant.

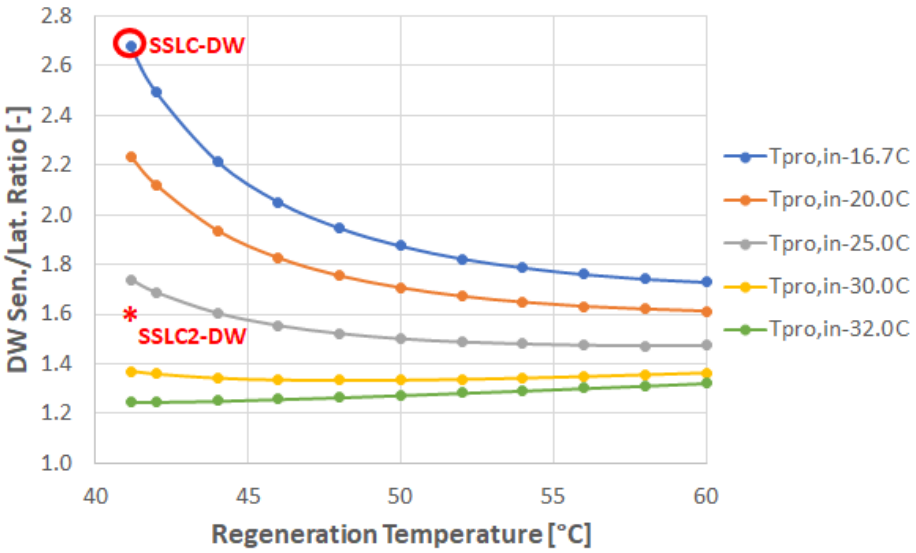

Figure 41: DW sensible to latent ratio at different inlet regeneration & process air temps.

A Second Law analysis was performed on the SSLC-DW system according to the approach discussed in Section 3.1.5. The Grassmann diagram depicts the total amount of work extracted from the SSLC-DW system (Figure 42). For simplicity, the desiccant wheel was not analyzed. However, this approach allowed evaluation of the effects of the desiccant wheel on the VCS components. Each component in the SSLC-DW system was responsible for a portion of the total exergy destruction ranging from 12.8% for the expansion valve to 23.0% in the condenser. The compressor and expansion valve losses accounted for nearly 1/3 of the total destroyed exergy (33.5%) while heat exchangers accounted for 41.2%. The remaining 25.4% represented the exergy efficiency of the system calculated by using Equation (3).

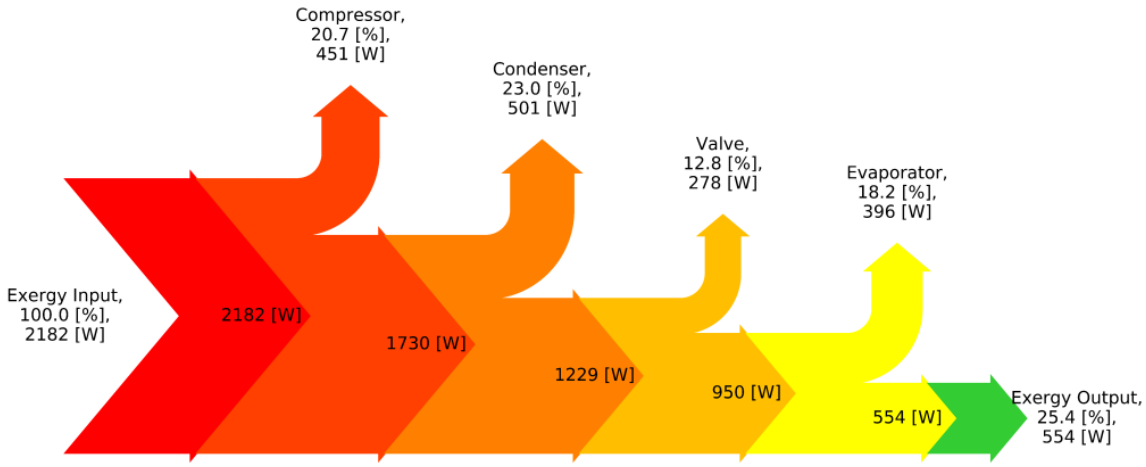

Figure 42: Grassmann diagram of the DW-assisted SSLC system.

The exergy of the SSLC-DW system compared to the baseline system are shown in Table 18. The exergy of all SSLC-DW components was higher than those of the baseline. The main increase of the destroyed exergy occurred in the heat exchangers due to their increased capacities. Thus, the exergy efficiency of the SSLC-DW system was lower despite the higher exergy input.

Table 18: SSLC-DW exergy compared to baseline.

	Baseline	SSLC-DW	Diff
Exergy Input [kW]	2.161	2.182	0.97%
Compressor [kW]	0.451	0.421	0.18%
Condenser [kW]	0.486	0.501	3.27%
Valve [kW]	0.277	0.278	0.61%
Evaporator [kW]	0.382	0.396	3.69%
Exergy Output [kW]	0.566	0.554	-2.04%
Exergy Efficiency [%]	26.2%	25.4%	-2.98

Based on the preceding results, a new DW assisted SSLC (SSLC2-DW) was proposed as shown in Figure 43. In this system, the DW is located at the evaporator inlet. This configuration would offer the following advantages. Firstly, the sensible to latent heat ratio of the DW would be lower because of higher process air inlet temperature as shown in Figure 41 (SSLC2-DW), reducing the additional heat load caused by the DW to the system. Secondly, the air temperature at the evaporator inlet would be higher because of the additional heat added to the process air by the DW. The higher air inlet temperature would increase the evaporating temperature and consequently reduce the compressor pressure ratio and compressor power. Thirdly, the increased evaporating temperature would increase the dew point temperature of the air at the evaporator outlet. Thus, condensation would not occur at lower air flow rates which would allow reduced evaporator air flow rate and consequently reduced evaporator fan power.

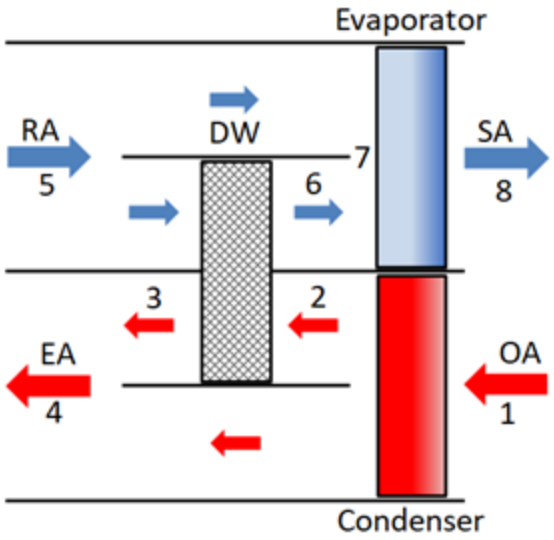

Figure 43: Airflow of DW-assisted SSLC2 system.

Figure 44 shows the compressor and total power at different air flow rates. It is obvious that the compressor power could decrease by slightly increasing the evaporator air flow rate. However, the decreased compressor power consumption barely affects the total power consumption of the system because of the increased evaporator fan power consumption. The effects of the regeneration temperature on the SSLC2-DW system were not investigated because according to Figure 41 no system improvement was expected at the 27°C process air inlet temperature.

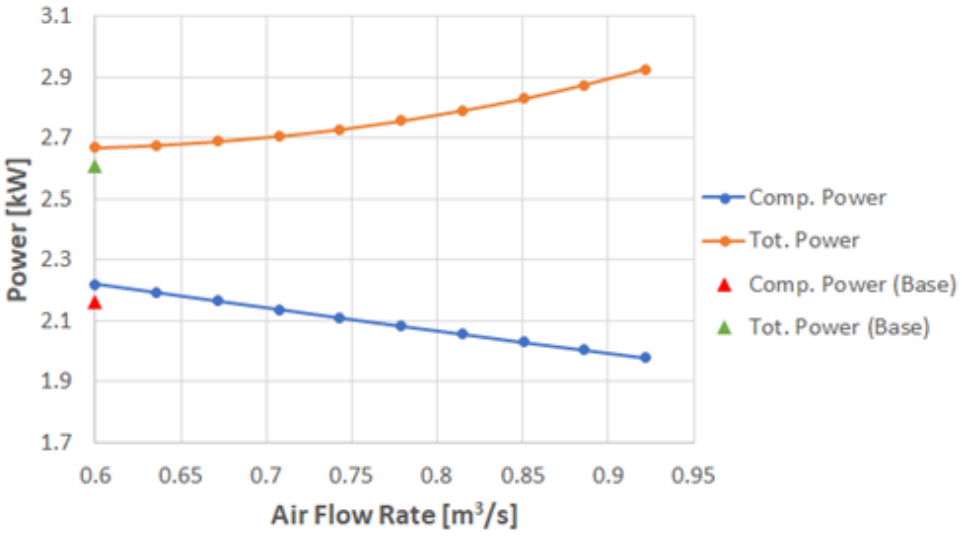

Figure 44: Power vs air flow rates of baseline & SSLC2-DW systems.

3.5.4. DW-Assisted SSLC System Findings

The modeled DW-assisted SSLC systems did not show improvement over the baseline due to the following:

1. The air flow rate was increased for the SSLC–DW system to avoid any condensation in the evaporator. In the SSLC2-DW, the evaporator flow rate needs to be increased to meet the total cooling load although no condensation is expected at the baseline level air flow rate. The increased evaporator air flow rate resulted in higher evaporator fan power which eliminated any reduction in compressor power and reduced the system COP. In previous studies, the conventional and SSLC systems were compared at the same evaporator air flow rates.
2. The SSLC analyses showed that the DW significantly increases the sensible heat of the cooling system. This additional sensible load needs to be removed by the evaporator which consequently would increase the compressor and/or evaporator fan power. In DW-assisted ACs, the additional sensible load is either removed by energy recovery wheels or used instead of reheating the supply air. The baseline system in this study did not use any recovery wheel nor any reheater.
3. For building ventilation, the outside air is either mixed with the return air or directly supplied to the space. A DW would be more efficient for the dehumidification of outside or mixed air which is usually hotter and has higher moisture content (higher humidity ratio). No ventilation was considered in the current study.
4. In previous studies, the DW-assisted SSLC systems were compared with the conventional AC with low evaporating temperatures (~7 °C). The increase of the evaporating temperature by few degrees (5-7 K) showed a decrease in the compressor power and consequently an increase in the COP. The evaporating temperature of the baseline system was already relatively high (~11.4 °C), and the small increase by 2.1 K did not show any significant system improvement.
5. Finally, the previous studies did not investigate the increase of the evaporator and condenser fan power consumption caused by the increased air pressure drop through the DW.

3.6. Variable Speed Compressor Concept

Based on input from Goodman, approximately 10% of the market for residential split AC systems employ inverter driven variable speed compressors in the outdoor unit. Lack of market adoption is related directly to the cost premium of the components compared to a single speed compressor system. It stands to reason that over time the cost of a variable speed compressor will fall, whether this is precipitated by increased adoption due to increased energy costs, or a technology evolution. Since a variable speed compressor and associated control algorithms could be combined with any design concept presented in this report, OTS considered the potential of this technology and conducted some preliminary analysis.

To map the potential of variable parameter operation the compressor utilized in the VapCyc® model of the baseline system was replaced with a suitable variable speed compressor by changing the set of 10 coefficients for the compressor model. Parametric runs were conducted in VapCyc® manipulating the compressor coefficients (compressor rpm), indoor unit (AHU) fan speed, as well as the outdoor unit air ambient conditions. The ambient temperatures for a range of bin temperatures were used based on the AHRI Standard 210/240 (AHRI, 2017).

The set speeds for the AHU fan and the compressor were normalized by the speeds from the baseline operating condition. This ratio for the fan speed is r_{fan}, which ranged from 0.47 to 1.10, and for the compressor speed the ratio is r_{comp} and ranged from 0.56 to 1.39. Results of the parametric runs are plotted in Figure 45, where color represents compressor speed ratio and the dot size represents fan speed ratio. The direction of change in increasing fan speed ratio is indicated with an arrow.

The HX and system performance parameters for capacity, condensation rate, and EER were normalized by the baseline system values. The compressor speed ratio, condensate ratio, and EER ratio of the baseline are indicated in Figure 45 with crossed black lines.

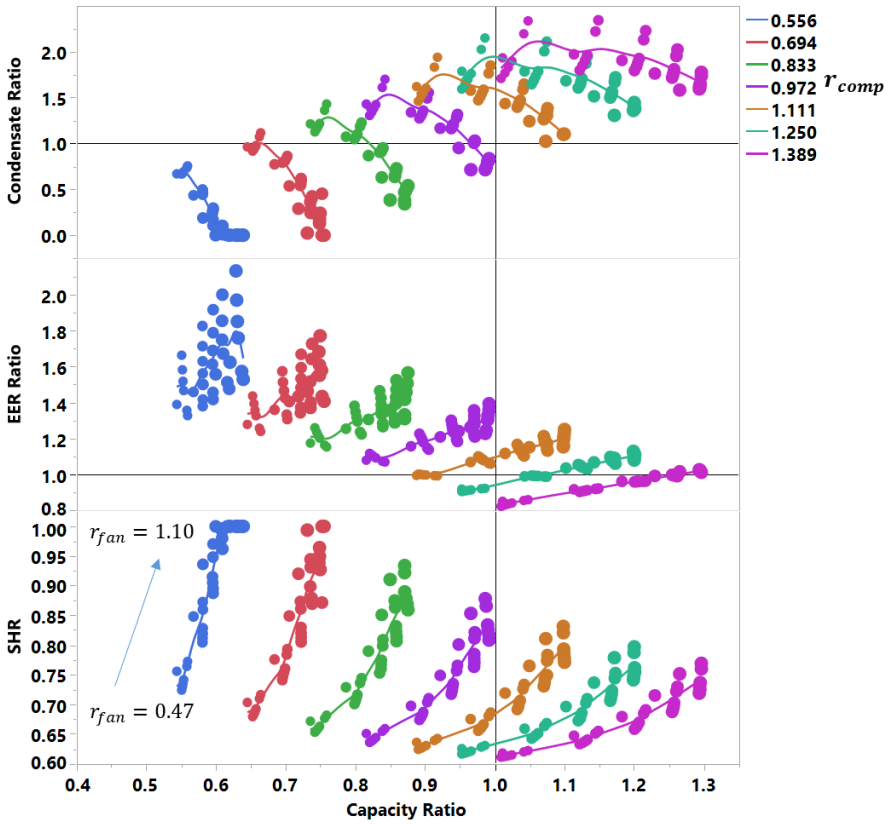

Figure 45: Map of variable speed VCS behavior.

Of course, manipulating the compressor speed has a strong effect on the capacity ratio. EER ratio values greater than one, the baseline, are desirable. Reduced compressor speed reduced capacity but also increased EER. At lower compressor speed ratios, manipulating the fan speed had a strong effect on SHR and condensate ratio, and to a lesser extent, the EER ratio. A candidate system with a variable speed compressor and fan(s) can operate at any region between points shown. If this candidate system could sense the temperature and humidity of the surroundings, then control algorithms could determine the settings for the compressor and fan speeds, and the system could adapt to the appropriate sensible and latent loads. Anytime system operation with an EER ratio greater than one would result in energy savings. The benefit is two-fold; besides energy savings, the system would improve comfort by better adapting to the loads.

A variable speed compressor and fan could be modulated to run at a high evaporation temperature for sensible-only cooling and only run at a lower evaporation temperature when latent cooling is needed. A high efficiency, sensible mode could be run most of the time in dry climates leading to energy savings.

Since this project primarily focused on the AHU and not the outdoor unit, further development was out of scope for the current effort. OTS recommends that the variable speed concept be paired with the proposed next generation AHU system configuration and studied further in future work.

4. Conclusions

OTS developed multiple concepts in several solution categories: ejector enhanced vapor compression cycles, desiccant assisted dehumidification, multi-evaporator SSLC, alternative AHU HX configurations, and variable speed compressor load following. A summary and discussion of key findings for each concept follows:

1) A hypothetical dual vapor compression system (VCS) SSLC concept was studied to inform alternative concepts and to determine best-case theoretical performance benefit. Results indicated this approach could achieve a maximum COP performance benefit on the order of 30%, while detailed analysis showed a COP performance benefit of 20%. However, significant system architecture changes are required with additional components, increased unit size, and increased cost.

2) Desiccant air conditioners offer a solution which meets humidity and temperature requirements via decoupling latent and sensible loads. A solid desiccant wheel (DW) formed from Ferroaluminophosphate Zeolite was proposed to act as a dehumidifier, allowing the vapor compression system to manage cooling function with a higher temperature evaporator. However, increased air flow rate was required to avoid condensation in the evaporator resulting in higher evaporator fan power which reduced the system COP. The DW significantly increased the sensible heat load leading to increased compressor power.

3) A SSLC system can utilize two evaporators, one with higher temperature to provide sensible cooling, and another with lower temperature to provide dehumidification. A traditional vapor compression cycle with dual evaporators has higher expansion losses which resulted in a 13.4% performance degradation in COP.

4) Alternative AHU HX configurations and designs are harmonious with the other concepts considered and play an important part of any next generation AHU design.

Properly optimized single slab HX designs instead of an A-coil led to:

- 44–49% reduction in material (aluminum)
- 47–60% less refrigerant charge
- Improved HX velocity distribution

5) The primary objectives of the Phase I project focused on the AHU, not the outdoor unit. However, OTS additionally framed a high-level system concept for a variable capacity AC enabled by ECM fans and a variable speed compressor. The variable capacity system concept is synergetic with any of the AHU solutions proposed above, but was considered beyond the scope of Phase I.

6) An ejector employed as an expansion device recovers expansion losses, boosts pressures, and facilitates a dual evaporator system. Four categories of ejector enhanced vapor compression cycles were investigated, leading to seven potential system concepts, with required component or configuration changes limited to the AHU. These seven cycles were screened for performance impact and two favorable cycles emerged: COS and DOS.

   Condenser outlet split (COS) and diffuser outlet split (DOS) ejector enhanced vapor compression cycles:

   System performance:
   - 4–8% increase in SEER (above 15 SEER baseline)
   - 9–11% increase in COP

   AHU performance:
   - 6–18% decrease in AHU exergy destruction

5. Degree to which Phase I has Demonstrated Technical Feasibility

In Phase I, Topic 9a: Next Generation Residential Air Handlers, Optimized Thermal Systems, Inc. (OTS) focused on improving AHU performance by minimizing HX approach temperature, finding opportunities to reduce air maldistribution, and focused on alternative system configurations which can more efficiently handle sensible and latent loads.

OTS developed multiple concepts in several solution categories: ejector enhanced vapor compression cycles, desiccant assisted dehumidification, multi-evaporator

SSLC, alternative AHU HX configurations, and variable speed compressor load following.

A next generation AHU integrating an ejector in the AHU refrigerant circuit is proposed. The ejector recovers expansion losses and lifts the pressure of the refrigerant that is returned to the compressor in the outdoor unit, thus reducing compressor power consumption. In this way the AHU plays a more active role in improved system performance.

Additionally, replacement of the traditional AHU A-coil with a single-slab HX is proposed. For use with the ejector enhanced cycle, a single-slab HX with dual-circuited evaporator and angled-slab configuration is desirable. The resulting improvement in air maldistribution can provide additional modest system level capacity and COP increases.

The following list summarizes status to targets for the proposed next generation AHU:

1) Exceeds the greater than 5% system energy efficiency increase target with the potential for 9 – 11% COP improvement.
2) Does not meet a greater than 25% AHU energy consumption reduction target, but reduces AHU losses by as much as 18%
3) Meets the physical size target (concept does not require increase in system size).
4) Meets cleaning targets (no anticipated changes required to cleaning intervals).
5) Moderate system first cost increase to be minimized with further research.

Generally, significant opportunity for energy consumption reduction within the AHU itself was not identified, especially on the order of a 25% or greater decrease. The primary energy-consuming components inside the AHU are the blower and motor, and parasitic power losses are a relatively small percentage of the overall losses in the system. However, with the COS or DOS ejector enhanced cycles, the AHU losses in the form of exergy destruction were reduced by up to 18%.

The recovery of expansion losses with an ejector further increases with natural refrigerants such as propane (R290), isobutane (R600a), or CO_2 (R744). Basic analysis showed a 2% additional increase in system COP with propane and 4% additional with isobutane, as compared to the baseline R410A.

With respect to system first cost, the ejector is an additional component and, as such, the addition increases the first cost of the AHU. This cost increase can be offset to some degree by the proposed HX design, which greatly reduced material and refrigerant charge. Estimates of costs based on current market rates, not representing actual costs to manufacture each of the components, showed the incremental cost of the next generation AHU is expected to be on the order of $80. This increase is well within the allowable cost increase the market will tolerate for favorable system upgrades.

Two of the targets were very difficult to assess during concept work in Phase I: improved system reliability; and little to no increase in susceptibility to damage, corrosion, or performance degradation during the product lifecycle. These targets should be addressed during Phase II as the design of the concept matures.

6. Anticipated Public Benefits

Through the efforts conducted in Phase I, OTS has identified a suitable design for a next generation residential AHU. This product is intended to reduce residential energy consumption attributed to the HVAC system as well as improve indoor comfort. The new design will not only serve the new construction market for single- and multi-family construction but can also serve as a retrofit unit for existing building stock.

The new solution is superior to conventional AHUs in that it leverages the benefits of an ejector and separates sensible and latent cooling needs. These enhancements allow for more efficient operation and better control of conditioned air outlet temperature and relative humidity.

While much research has been conducted on use of ejectors in refrigeration, and to a lesser extent, air-conditioning applications, their primary application today is in large capacity supermarket refrigeration applications, typically with CO_2 as the refrigerant where expansion losses are otherwise high. While ejectors can be beneficial in other applications and with other refrigerants, their commercial availability is poor, hindering adoption and integration into new systems. It is anticipated that future work on this topic will lead to potentially novel ejector design, commercialization of the proposed AHU concept, and help to lead to wider adoption of energy saving ejector technology.

Electric powered central heat pump and air-conditioning systems in the U.S. are projected to consume nearly 2,200 trillion Btu and 89 Mt CO2 by 2023 (Baseline

Energy Calculator, 2020), which is approximately 25% of the HVAC contribution for residential applications, nationwide. With the potential for 9–11% improvement in COP, an ejector enhanced next generation AHU can have considerable impact in the energy consumption outlook.

In 2019 alone, there were more than 8.4 million air conditioner and heat pump purchases across the U.S. (AHRI, 2020). Even if the new technology captured only a fraction of the market, sales would still result in several million units each year.

Although the energy efficiency improvements of the next generation AHU described in this report met the > 5% system target, with modifications limited to the AHU only, they did not approach the dual VCS SSLC benefit of 20%. There is opportunity to improve the ejector enhanced cycles by driving the low temperature evaporator towards a more latent HX, perhaps with a novel air-to-air HX. System concepts that incorporate innovative heat exchanger designs and expand beyond the AHU, to the outdoor unit as well, offer possibilities to reach energy efficiency gains aspiring to the theoretical SSLC maximum benefit. Additionally, such systems offer future opportunities in terms of novel intellectual property.

7. References

AHRI (2017). ANSI/ARI Standard 210/240 for Performance Rating of Unitary Air-Conditioning and Air-Source Heat Pump Equipment. Air-Conditioning and Refrigeration Institute, Arlington, VA.

Air-Conditioning, Heating, & Refrigeration Institute (AHRI). AHRI Releases December 2019 U.S. Heating and Cooling Equipment Shipment Data. http://www.ahrinet.org/App_Content/ahri/files/Statistics/Monthly%20Shipments/2020/February_2020.pdf

Al-Alili, A., Hwang, Y., Radermacher, R., and Kubo, I. (2012). A High Efficiency Solar Air Conditioner Using Concentrating Photovoltaic/Thermal Collectors. Applied Energy Vol. 93., 138-147.

Al-Alili, A., Hwang, Y., Radermacher, R., and Kubo, I. (2015). Performance of a Desiccant Wheel Cycle Utilizing New Zeolite Material: Experimental Investigation. Energy Vol. 81., 137-145.

ASHRAE 139 (2007). Methods of Testing for Rating Desiccant Dehumidifiers Utilizing Heat for Regeneration Process. American Society of Heating, Refrigerating and Air Conditioning Engineers.

ASHRAE (2020). ASHRAE Terminology: A Comprehensive Glossary of Terms for the Built Environment. https://xp20.ashrae.org/terminology/

Baseline Energy Calculator (2020). U.S. Department of Energy, Building Technologies Office, Office of Energy Efficiency & Renewable Energy. https://scout.energy.gov/baseline-energy-calculator.html

De Antonellis, S., Intini, M., and Joppolo, C.M., (2015). Desiccant Wheels Effectiveness Parameters: Correlations Based on Experimental Data. Energy and Buildings Vol. 103, pp. 296-306.

ERTC (2014). About Ejector Refrigeration Technologies. Odessa State Academy of Refrigeration, Ukraine. http://www.ertc.od.ua/en/about_ert_en.html

Goetzler, W., Zogg, R., Young, J., & Schmidt, J. (2012). Building Technologies Office Energy Savings Potential and Demonstration Opportunities for Residential Building Heating, Ventilation, and Air Conditioning Systems.

Goodman Manufacturing Company, L. P. (2019). AVPTC Product Specification. https://www.goodmanmfg.com/docs/librariesprovider6/default-document-library/ss-gavptc.pdf

Hwang, Y., Kuwabara., O., Ling, J., and Radermacher, R. (2010). Enhancement of the Separate Sensible and Latent Cooling Air-Conditioning Systems. Paper 1068. International Refrigeration and Air Conditioning Conference at Purdue.

Jiang, H., Aute, V., and Radermacher, R. (2006). CoilDesigner: a General-Purpose Simulation and Design Tool for Air-to-Refrigerant Heat Exchangers. International Journal of Refrigeration Vol. 29., 601-610.

Kim, S., Jeon, Y., Chung, H. J., & Kim, Y. (2018). Performance optimization of an R410A air-conditioner with a dual evaporator ejector cycle based on cooling seasonal performance factor. Applied Thermal Engineering, 131, 988–997.

Klein, S.A., (2020). Engineering Equation Solver. http://fchartsoftware.com/ees/

Kornhauser, A. A. (1990). The Use of an Ejector as a Refrigerant Expander. Proceedings of the 1990 USNCR/IIR-Purdue Refrigeration Conference, 10–19. West Lafayette, IN.

Lawrence, N., & Elbel, S. (2013). Theoretical and practical comparison of two-phase ejector refrigeration cycles including First and Second Law analysis. International Journal of Refrigeration, 36(4), 1220–1232.

Lee, W. H., Kim, Y. J., Kim, M. S., & Cho, K. S. (2000). Experimental Study on the Performance of Dual-Evaporator Refrigeration System with an Ejector. International Refrigeration and Air Conditioning Conference., Paper 503.

Li, Z., Aute, V. C., & Ling, J. (2018). Tube-Fin Heat Exchanger Circuitry Optimization for Multiple Airflow Maldistribution Profiles.

Ling, J., Kuwabara., O., Hwang, Y., and Radermacher, R. (2011). Experimental Evaluation and Performance Enhancement Prediction of Desiccant Assisted Separate Sensible and Latent Cooling Air-Conditioning Systems. International Journal of Refrigeration, Vol. 34, pp. 946-957.

Mitsubishi Plastics (2010). Zeolitic Water Vapor Adsorbent AQSOA™. http://www.aaasaveenergy.com/products/001/desiccant/index.html

Nóbrega, C., and Brum, N. (2014). Desiccant-Assisted Cooling. Springer Verlag London. ISBN 978-1-4471-5565-2.

Radermacher, R., & Hwang, Y. (2005). Vapor Compression Heat Pumps with Refrigerant Mixtures.

Richardson, D., & Jiang, H. (2002). Optimization of vapor compression systems via simulation. International Refrigeration and Air Conditioning Conference, (March).

Tomasek, M.-L., & Radermacher, R. (1995). Analysis of a domestic refrigerator cycle with an ejector. ASHRAE Transactions, 101, 1431–1438.

U.S. Energy Information Administration (2015). 2015 Residential Energy Consumption Survey: Energy Consumption and Expenditures Tables. https://www.eia.gov/consumption/residential/data/2015/c&e/pdf/ce3.1.pdf

Wang, S. K. (2001). Handbook of Air Conditioning and Refrigeration (Second edition).

Wang, X., Yu, J., Zhou, M., & Lv, X. (2014). Comparative studies of ejector-expansion vapor compression refrigeration cycles for applications in domestic refrigerator-freezers. Energy, 70(June 2014), 635–642.

Yashar, D. A., & Cho, H. H. (2007). NISTIR 7474: Air-Side Velocity Distribution in Finned-Tube Heat Exchangers. Gaithersburg, MD.

Yashar, D. A., & Domanski, P. A. (2009). ARTI Report No. 07010-01: Particle Image Velocimetry Measurements And CFD-Based Predictions of Air Distribution at Evaporator Inlet and Outlet. Gaithersburg, MD.

Yin, P., & Pate, M. B. (2019). An energy and life-cycle cost comparison of residential PSC and ECM blower systems operating at excess pressures due to restrictive ducts. Journal of Building Engineering, 22, 305–313.

8. NDAA of 2019 Annual Technical or Business Assistance Report

Vendor name: Goodman Manufacturing Company, L.P. (Goodman)

Type of services:

- Commercialization consulting

Benefits of the service(s) provided:

Goodman has been designing and manufacturing HVAC equipment for more than thirty years, with experienced technical and marketing staffs. They have a strong perspective on barriers to new product introduction in a cost-sensitive and risk adverse industry. Goodman also has state of the art manufacturing facilities and manufacture many of their own components and subsystems.

Results of the service(s) provided:

Goodman provided input on the selection of a suitable baseline AHU and supplied an AHU to OTS. Goodman provided computational fluid dynamics results and baseline heat exchanger and vapor compression cycle models for OTS review. Goodman reviewed technical results and provided input on areas of focus, concern, and next steps on both technical and commercialization topics to assist OTS planning for Phase II.